ACS APPLIED BIO MATERIALS

www.acsabm.org Article

# Surface Modification of Polypropylene Mesh with a Porcine Cholecystic Extracellular Matrix Hydrogel for Mitigating Host Tissue Reaction

Reshmi Raj, Sachin J. Shenoy, Manjula P. Mony, Kanakarajan V. Pratheesh, Reshma S. Nair, Chandrika S. Geetha, Praveen K. Sobhan, Chandramohanan Purnima, and Thapasimuthu V. Anilkumar*

Cite This: *ACS Appl. Bio Mater.* 2021, 4, 3304–3319 Read Online

ACCESS | Metrics & More | Article Recommendations | Supporting Information

**ABSTRACT:** Polypropylene (PP) meshes are widely used for repairing skeletal muscle defects like abdominal hernia despite the chances of undesirable pro-inflammatory tissue reactions that demand revision surgeries in about 45% of cases. Attempts have been made to address the problem by modifying the mesh surface and architecture. These procedures have yielded only incremental improvements in the management of overall postoperative complications, and the search for a clinically viable therapeutic strategy continues. This study deployed a tissue engineering approach for mitigating PP-induced adverse tissue reaction by dip-coating the mesh with a hydrogel formulation of the porcine cholecystic extracellular matrix (CECM). The biomaterial properties of the CECM hydrogel-coated PP (C-PP) meshes were studied and their biocompatibility was evaluated by *in vitro* and *in vivo* tests based on ISO standards. Further, the nature of tissue reactions induced by the hydrogel-coated mesh and a commercial PP hernia repair graft was compared in a rat model of partial-thickness abdominal wall defect. Histomorphologically, in comparison with the PP graft-induced tissue reaction, C-PP caused a favorable graft-acceptance response characterized by reduced numbers of pro-inflammatory M1 macrophages and cytotoxic lymphocytes. Remarkably, the differential inflammatory response of the C-PP graft-assisted healing was associated with a fibrotic reaction predominated by deposition of type I collagen rather than type III collagen, as desired during skeletal muscle repair. It was concluded that the CECM hydrogel is a potential biomaterial for surface modification of polymeric biomedical devices.

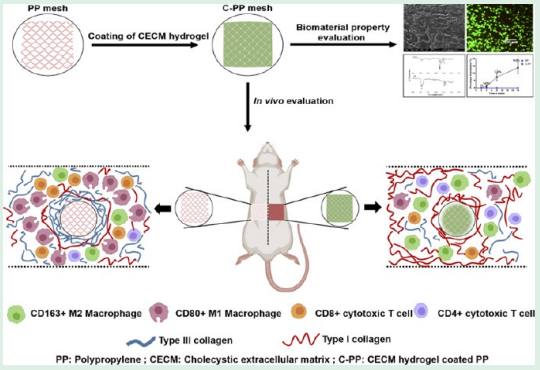


**KEYWORDS:** *hernia repair, biomaterial, biocompatibility, M1 macrophage, cytotoxic lymphocytes, type I/type III collagen ratio*



## 1. INTRODUCTION

Polymeric meshes are commonly used for reinforcing mechanical strength to the damaged skeletal muscle for repairing abdominal hernia,[1] which is essentially translocation of abdominal organs through a compromised musculoaponeurotic barrier.[2] The standard polymeric material used for abdominal hernia repair is polypropylene (PP).[3] Following implantation, PP meshes trigger a chronic inflammatory response predominated by foreign body reaction and formation of a dense fibrous tissue capsule around the mesh material.[4] Whereas such reactions are inevitable around any non-degradable biomaterial, inadequacies in the fibrous tissue reaction often lead to shrinkage, erosion, decreased tissue compliance, and graft rejection, demanding revision surgeries in about 45% of cases.[5,6] Several studies have attempted to address the issue of graft rejection and proposed different strategies for mitigating the PP mesh-induced inadvertent pro-inflammatory reaction in the skeletal muscle. The common strategies are creating alterations in the mesh composition and optimizing the pore size.[7] Nevertheless, these strategies have yielded only incremental improvements in the overall postoperative complications.[8]

Recently, surface coatings of PP mesh implants with bioactive molecules have gained increased attention, which brings benefit at least in two generic ways by modulating implant degradation and mitigating the nature of inflammation.[9] In this context, xenogeneic extracellular matrices (ECMs) prepared by decellularization of the mammalian organ/tissue have been proposed as a surface-coating material for the mitigation of the graft-induced reactions.[10] Although Faulk et al. (2014)[11] attempted to use a porcine dermal ECM hydrogel for surface

Received: December 19, 2020
Accepted: February 23, 2021
Published: March 10, 2021

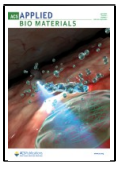

coating, no clinical utility has been proposed so far. There could be several reasons for not finding any clinical utility for mammalian-ECM hydrogel-coated PP (C-PP) meshes. Biomaterial properties and potential clinical utility of mammalian-ECM hydrogels depend not only on the source organ but also on the hydrogel preparation method. Faulk et al. deployed the conventional Freytes method[12] for preparing the mammalian-ECM hydrogel, which yields soft ECM hydrogels that have high degradation rates and a low storage modulus of 5−10 Pa at 1 Hz.[13] Such a hydrogel preparation probably has limitations as a surface-coating material for a device that demands high mechanical strength and a longer implantation period.

We have reported a biocompatible[14,15] porcine cholecystic ECM (CECM) for tissue engineering applications.[16,17] The biomolecular composition of the CECM has been reported earlier.[18] It contains collagen, glycosaminoglycans, elastin, and many growth factors crucial for stimulating tissue remodeling responses.[16] As a biomaterial for graft-assisted healing, lyophilized sheet forms of the CECM promoted faster healing of skin excision,[19] burn,[20] and lacerated wounds in animal models.[17] Experiments have shown that as a skeletal muscle graft, in a rat hernia repair model, the lyophilized sheet form of the CECM promoted M2 macrophage-predominated anti-inflammatory reaction.[15] Recently, a hydrogel formulation of the CECM was prepared by free radical polymerization with poly(ethylene glycol)diacrylate (PEGDA). The prepared CECM hydrogel had a significantly reduced degradation profile and tunable mechanical strength (depending on the concentration of the gelling agent) and was found suitable for skeletal muscle tissue engineering.[21] However, the possibility of using the above CECM hydrogel as a PP mesh surface modification material for modulating the host response has not been explored. Therefore, as part of this study, an empirical dip-coating method was identified for the surface modification of a PP mesh. However, the primary objective of this study was to evaluate the nature of the tissue reaction induced by the CECM hydrogel C-PP mesh in a rat model of partial-thickness abdominal hernia repair involving skeletal muscle damage. The second objective of this study was to evaluate the biomaterial properties of the C-PP mesh as a biomedical device.

## 2. MATERIALS AND METHODS

**2.1. Preparation and Coating of the CECM Hydrogel onto PP Mesh.** The base material, lyophilized sheets of the CECM (about 150 $\mu$m thick), was prepared by a non-detergent/enzymatic method as previously described[16] by mechanical delamination after *ex situ* incubation of the source organ with 10% neutral buffered formaldehyde (48 ± 24 h) for controlled cross-linking of biomolecules.[17]

The preparation of the CECM hydrogel was essentially a three-step process involving solubilization, functionalization, and gelling.[21] In the first step, the lyophilized sheet of the CECM was powdered in a freezer mill (Spex SamplePrep, 6770, USA) to form CECM powder, enzymatically solubilized with pepsin−HCl (Sigma-Aldrich, USA) solution (1:10 w/w), and subsequently neutralized to physiological conditions (pH 7.4) with 0.1 N NaOH and 10× PBS. In the second step, the CECM was functionalized with acrylate groups using 1-ethyl-3-(3-dimethyl aminopropyl)carbodiimide (EDC) (2 mM) and *N*-hydroxy succinimide acrylate (NHS-acrylate) (4 mM) solution. The weight ratio of the CECM to EDC−NHS acrylate solution was 1:0.09 (w/w). The unreacted EDC−NHS−acrylate components were removed by centrifugal filtration (Amicon Ultra-4 centrifugal filter device, a nominal molecular weight limit of 3 kDa) at 5000 rpm (three times). The acrylate-modified CECM was the pre-gel solution. In the third step, the acrylate-modified CECM pre-gel solution and the gelling agent PEGDA (2 mg/mL) (Sigma-Aldrich, USA, $M_n$ = 700) were mixed in a weight ratio of 1:0.08 (w/w) over the PP mesh to achieve the dip-coating as described below.

The dip-coating was done as described previously[10] on a commercially available monofilament non-absorbable PP mesh, Trulene (Sutures India), which was also used as the reference material or the predicate device. Briefly, 2 × 2 cm pieces of the pre-cut PP mesh were immersed in a square plastic dish containing 25 mL of acrylate modified CECM/PEGDA solution. Gelation was induced by adding ammonium persulphate (0.04 M, 9 mg/mL) and ascorbic acid (0.1 M, 17.6 mg/mL), followed by incubation at 37 °C for 45 min. The CECM hydrogel C-PP meshes were then washed five to eight times in sterile PBS to remove the toxic unreacted monomeric form of PEGDA and persulphates. The hydrogel-coated meshes were then lyophilized and terminally sterilized by exposure to UV light (at 254 nm wavelength) inside a biosafety cabinet (Kleanzone devices, India) for 30 min.

**2.2. Biomaterial Properties of the C-PP Mesh.** Scanning electron microscopy (FEI, Quanta 200, USA; operating voltage 10 kV) was performed on lyophilized samples of PP and C-PP meshes, after sputter-coating with gold ($n$ = 2/group).

Fourier transform infrared spectroscopy (FTIR, JASCO 4200, Easton, USA) was used to characterize the chemical composition of the coated and uncoated PP meshes in the infrared range of 4000−400 $cm^{-1}$, with the attenuated total transmittance mode, at room temperature ($n$ = 2/group).

Mechanical properties of the C-PP mesh were studied using a universal testing machine (Instron model 3345, United Kingdom) with a 100 N load cell at a speed of 5 mm/min. Based on the recorded force−displacement−time data, the maximum extension until the break was calculated ($n$ = 4/group).

**2.3. Nonenzymatic Degradation of the C-PP Mesh.** The degradation behavior of the C-PP mesh (dimension: 2 × 2 cm, weight: 28 mg) and CECM hydrogel (8 mg) was studied in comparison with that of the PP mesh (dimension: 2 × 2 cm, weight: 20 mg). Samples ($n$ = 4) from each group were weighed and then soaked in 5 mL of sterile PBS at 37 °C. At predetermined intervals (2, 4, 8, and 16 weeks), the samples were removed and lyophilized for 16 h, and their weights were recorded. Degradation was determined by the sample weight loss[22]

$$\text{degradation (\%)} = \frac{W_i - W_d}{W_i} \times 100$$

($W_i$ and $W_d$ are the initial and degraded dry weights of the meshes, respectively). Extracts of the degraded mesh materials were analyzed by a UV−visible spectrophotometer (Varian Cary 100. 9.0, US) to know the chemical nature of the degradation products at 100−900 nm wavelength.

**2.4. *In Vitro* Biocompatibility Evaluation of the C-PP Mesh.** Biocompatibility of the C-PP meshes was assessed using the C2C12 mouse skeletal myoblast cell line (ATCC CRL1772, USA) by using the commercial PP meshes as the reference material and the CECM hydrogel was used as a control. In addition to this, cells cultured on tissue culture plastic were regarded as a positive reference control. The cell culture medium was Dulbecco's modified Eagle's medium with high glucose (Sigma-Aldrich, USA) for all experiments.

*2.4.1. Live/Dead Staining.* Cell viability was assessed by a routine live/dead staining procedure using C2C12 cells ($1 \times 10^3$ cells per well), which were cultured on the test materials in a four-well chamber system and incubated for 24 and 48 h in a cell culture medium. The viability of C2C12 cells on the test materials was determined by staining with fluorescein diacetate (Sigma-Aldrich, USA) (10 mg/mL) and propidium iodide (Sigma-Aldrich, USA) (10 mg/mL) and examining under a fluorescence microscope (Leica DMI 6000B) ($n$ = 3/group). The percentage viability of C2C12 cells was quantified using ImageJ software (NIH, USA).

*2.4.2. Phalloidin Staining.* Skeletal myoblast C2C12 cells were cultured in the chambered cover glass (Thermo Scientific Nunc Lab-Tek) at a density of $1 \times 10^3$ cells per well and incubated for 24 and 48 h in a cell culture medium. After the incubation, the medium was removed, and the cells were washed with PBS. The cells were then fixed in 1.2% paraformaldehyde at room temperature for 15 min and


https://dx.doi.org/10.1021/acsabm.0c01627
ACS Appl. Bio Mater. 2021, 4, 3304−3319

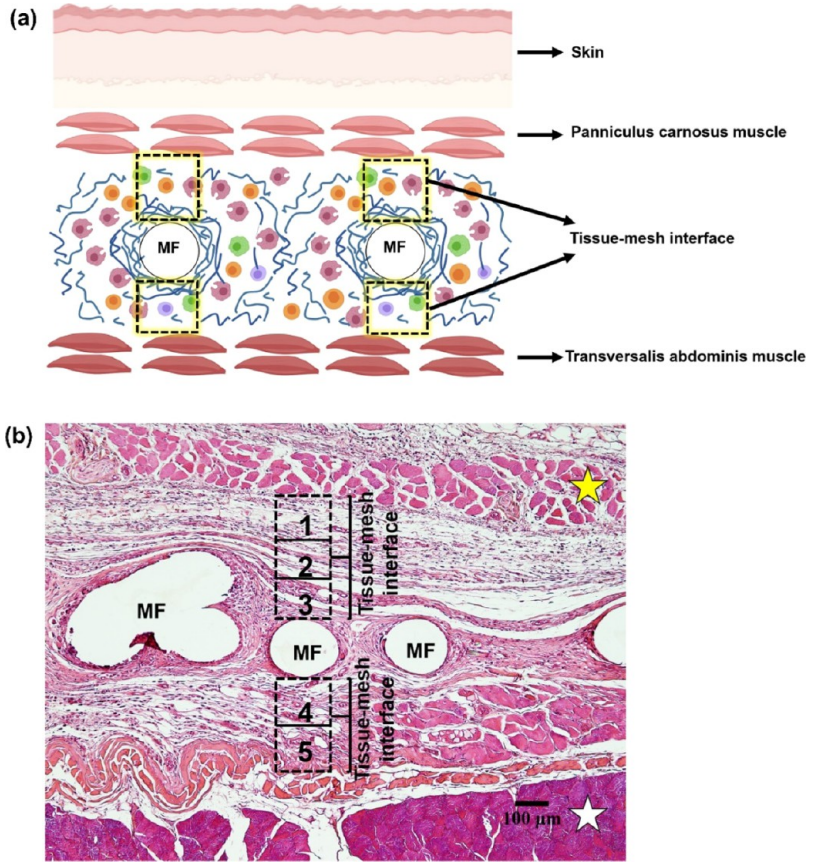


**Figure 1.** Image sampling plan adopted for histomorphometry. Schematic diagram (a) and a representative photomicrograph (hematoxylin and eosin stains) showing the sampling area at the tissue−mesh interface (dotted boxes, marked 1−5) selected for histomorphometry, between the mesh fiber (MF) and normal panniculus carnosus (yellow star) and transversalis abdominis muscle (white star).

permeabilized with 0.1% Triton X-100 for 1 min at room temperature. The permeabilized cells were stained with 5 $\mu$g/mL (1:100 dilution) fluorescein isothiocyanate-conjugated phalloidin (Sigma-Aldrich, USA) for 40 min and Hoechst 33342 stain for 5 min at room temperature in dark. The cells were then observed under a fluorescence microscope (Leica DMI 6000B) ($n$ = 2/group).

*2.4.3. Cell Cycle Analysis.* Cell cycle analysis was performed using propidium iodide (Sigma-Aldrich, USA) staining, as followed routinely.[23] Briefly, 1 × $10^4$ C2C12 myoblast cells were cultured in a six-well plate and incubated for 24 h to develop confluence; test materials (C-PP, PP, and CECM hydrogel) were placed carefully on the cell monolayer and incubated for a further period of 24, 48, or 72 h. The cells were then harvested and spun down for 5 min at 2000 rpm. The supernatant was removed, and the cells were fixed in 1 mL of ice-cold 70% ethanol overnight at −80 °C. The fixed cells were washed with 1 mL of PBS and treated with 500 $\mu$L of 1 mg/mL DNase-free RNase A (Sigma-Aldrich, USA) for 30 min at 37 °C. The RNase A-treated cells were stained with 200 $\mu$L of 1 mg/mL propidium iodide. The percentage of G0-G1, S, and G2-M cells, based on the DNA content, was then calculated using a fluorescence-activated cell sorter (BD Biosciences) ($n$ = 1/group).

*2.4.4. (3-(4,5-Dimethylthiazol-2-yl)-2,5-diphenyl)tetrazolium Bromide (MTT) Assay.* In addition to the live/dead staining, the biocompatibility of C2C12 skeletal myoblasts was studied by a "test on extract" method based on ISO 10993-5 (2009)[24] using MTT assay at 24, 48, and 72 h. The extracts of test materials were prepared using a cell culture medium without serum as the extraction vehicle at 72 ± 1 h at 50 ± 2 °C. Briefly, 1 × $10^3$ cells were cultured on a 24-well cell culture plate and incubated for 24 h at 37 °C with 5% $CO_2$. Then, the medium was replaced with the extracts of the test materials and incubated for further 24, 48, and 72 h. The control cells were incubated with the cell culture medium and 10 $\mu$L of MTT solution (5 mg/mL) for 3 h at 37 °C, and the absorbance was read at 570 nm (Biochrom ASYS UVM 340, Germany) ($n$ = 3/group).

**2.5. Biological Evaluation of the C-PP Mesh in Rats.** All animal experiments were designed and conducted as recommended in ISO 10993-Part 6 (2016),[25] with the approval of the Institutional Animal Ethics Committee of the host institution (SCT/IAEC/267/2018/95). Young male adult Sprague-Dawley rats (250−300 g) were used for the study. Animals were kept at standard laboratory conditions of the host institution (temperature of 22 ± 3 °C, humidity 30−70%, 12 h day/light cycle, and *ad libitum* access to feed and water). Sixteen rats were randomized by body weight into four groups ($n$ = 4) for implanting PP and C-PP meshes.

A partial-thickness abdominal wall defect (Figure S1) was created in the rats with minor modifications from the rat model reported previously.[15] The rats were anesthetized with ketamine hydrochloride (Neon Laboratories Limited, India) (80 mg/kg) and xylazine hydrochloride (Indian Immunologicals Limited, India) (10 mg/kg) by intramuscular injection. The general anesthesia was maintained by 1% isoflurane inhalation. A ventral midline skin incision was made in the abdominal region, and a 1 × 1 cm partial-thickness para-median defect was created on the left and right side of the *linea alba* by removing the internal and external oblique muscles, leaving the transversalis fascia and peritoneum intact. The defects were repaired by grafting a 2 × 2 cm PP mesh (on the left of the animal) or C-PP mesh (on the right of the animal) centered over the defect area, (overlay method) with interrupted 4-0 Prolene (Non-absorbable Surgical Suture U.S.P., Healthium Medtech, India) sutures. The skin was closed using a 3-0 Mersilk nylon suture in a horizontal mattress pattern over the implant (Figure S1). The post-surgical trauma was monitored and managed by appropriate veterinary care with the administration of ceftriaxone (20 mg/kg, intramuscular) and meloxicam (0.5 mg/kg, intramuscular) for three days post-surgery.


https://dx.doi.org/10.1021/acsabm.0c01627
ACS Appl. Bio Mater. 2021, 4, 3304−3319

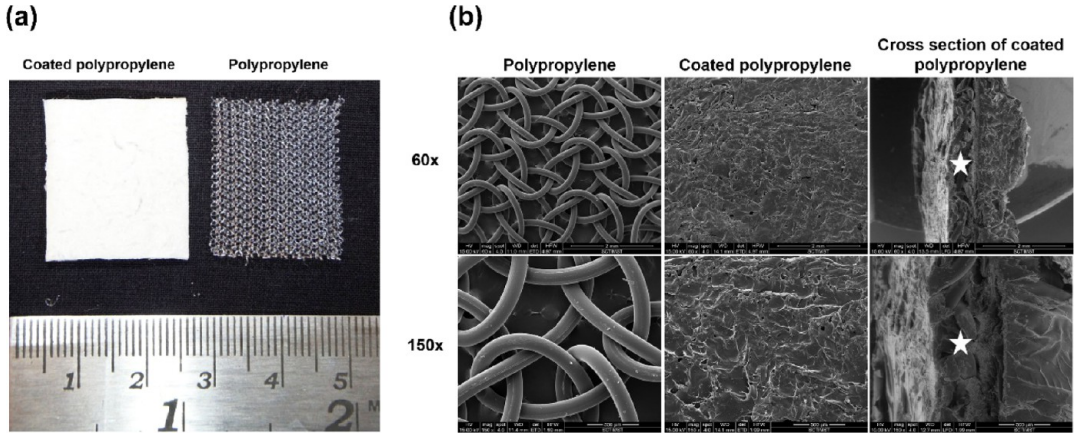


**Figure 2.** Macroscopic appearance and scanning electron micrographs of the mesh devices. (a) Macro photographs of a coated and an uncoated polypropylene mesh. (b) Scanning electron micrographs of a PP and a C-PP mesh at a magnification of 60× and 150×, $n = 2$. The white star indicates polypropylene in the cross-sectional view of the C-PP mesh, showing uniform coating into the knits of mesh fibers. PP: polypropylene; C-PP: CECM hydrogel-coated polypropylene mesh.

Four rats in each group were humanely killed in a $CO_2$ chamber at 2, 4, 8, and 16 weeks post-implantation (WPI). The implant site was identified by the presence of non-absorbable sutures. The abdominal wall including the implanted area was excised with the adjacent host native tissue, lifted gently, and examined macroscopically on both the implant site and peritoneal surface for the extent of vascularity. Potential complications such as infection, abscess, hernia, fistula, adhesion, seroma, hemorrhage, encapsulation, graft shrinkage, graft loss, or failed graft incorporation were recorded, if any. The implant with the surrounding native muscle (about 2 cm), at least 0.5 cm as the margin, was retrieved *en bloc* and fixed in 10% neutral buffered formalin for histomorphology and immunohistochemistry.

*2.5.1. Histotechnology, Histomorphology, and Histomorphometry.* Tissue bits were processed in an automated semi-enclosed bench top tissue processor, Leica TP1020 (Leica Biosystems, Germany), and embedded in paraffin wax. Tissue sections (4 $\mu$m thickness) were prepared using a semi-automated rotary microtome (RM2255, Leica Biosystems, Germany). Sections were stained routinely with Harris's hematoxylin and eosin (H&E) stain for histomorphology, Masson's trichrome for collagen deposition, and Herovici's stain for type I/type III collagen.[26]

All histomorphological and morphometric evaluations were carried out under the direct supervision of a veterinary pathologist. In histology sections, the mesh fibers were identified as round or oval-shaped vacant spaces in the damaged oblique skeletal muscle (internal and external oblique muscles) region between the panniculus carnosus and transversus abdominis muscles. Approximately 60% of these mesh fibers were found as coalescing groups constituting two−four fibers. Wherever quantitative data were collected, a uniform sampling plan (Figure 1) was followed, except for the determination of fibrotic capsule thickness around mesh fibers. Images of five non-coalescing mesh fibers were selected in tissue sections, and all the available high power (40×) microscopic fields (3−5) between the mesh fiber and normal tissue (skeletal muscle) were captured for the histomorphometry evaluation. The coalescing groups of fibers created a wide disparity in the tissue reaction between mesh fibers. Moreover, the consulted international standard demanded only an evaluation of the nature of the reaction between the biomaterials and healthy tissue. Therefore, quantitative evaluation of the tissue reaction between mesh fibers was avoided, except for evaluating the thickness of the fibrous capsule around mesh fibers.

Quantification of all histomorphometry evaluations was performed using Image-Pro version 3DS6.1 software (Media Cybernetics, Silver Spring MD). The number of cells in H&E and immunostained tissue sections were counted manually for ensuring accuracy in the identification of cell types. Quantification of fibrosis and differential distribution of type I and type III collagen were performed using stereology from Masson's trichrome and Herovici's stained sections, respectively.

An alternate sampling plan was considered for determination of fibrous capsule thickness. The determination of fibrous capsule thickness was measured by estimating the average thickness of the capsule from four different sites (3, 6, 9, and 12 o'clock positions) of five non-coalescing mesh fibers (Figure S2).

*2.5.2. Evaluation of Local Biological Effects after Implantation.* Local tissue reaction induced by the C-PP mesh was evaluated based on the ISO Standard 10993-Part 6 (2016),[25] and the commercial PP mesh (Trulene) was used as the predicate device or the reference biomaterial. In each H&E-stained histology section, the following parameters were studied: the number of inflammatory cells (neutrophils, plasma cells, lymphocytes, and macrophages), the number of foreign body giant cells, the severity of necrosis, the extent of neovascularization, the extent of fibrosis, and the extent of fatty infiltration in the designated areas as per the sampling plan (Figure 1). The average semi-quantitative score was then calculated as [(subtotal-I × 2) + subtotal-II], where subtotal-I is the sum of scores for neutrophils, lymphocytes, plasma cells, macrophages, giant cells, and severity of necrosis, and subtotal-II was the sum of the scores for neovascularization, fibrosis, and fatty infiltration. The difference of the average semi-quantitative score for the test material (C-PP) from the reference material (PP) was designated as the reactivity score for the C-PP mesh, as described in the standard.

*2.5.3. Immunohistochemistry.* Lymphocytes in the reaction zone were detected using antibodies against CD4 (Clone EPR19533, 1:100 dilution, catalogue no: ab183686, Abcam) and CD8 (Clone OX-8, 1:400 dilution, catalogue no: ab33786, Abcam) antigens. Macrophages in the reaction zone were detected by using antibodies against CD68 (Clone C68/684, 1:100 dilution, catalogue no: ab201340, Abcam), CD80 (Rabbit polyclonal, 1:100 dilution, catalogue no: ab215166, Abcam), and CD163 (Clone EPR19518, 1:600 dilution, catalogue no: ab182422, Abcam) antigens. Angiogenesis at the reaction zone was studied using antibodies against CD31 (Clone PECAM1, 1:400 dilution, catalogue no: NB100-2284, Novus Biologicals) and $\alpha$-smooth muscle cell actin (ASMA) (Clone B4, 1:300 dilution, catalogue no: sc53142, Santa Cruz Biotechnology) antigens. The presence of proliferating cells in the vicinity of the graft was detected with an antibody against the proliferating cell nuclear antigen (PCNA) (Clone PC10, 1:400 dilution, catalogue no: sc-56, Santa Cruz Biotechnology). The presence of fibroblasts in the reaction zone was identified by staining for vimentin (Clone VP-V684, 1:100 dilution, catalogue no: L103325, Vector Laboratories). Myofibroblasts in the reaction zone were also detected by immunostaining for ASMA. Individual cells other than those in blood vessels found positive for ASMA immunostaining were considered as myofibroblasts. Tissue sections treated without the corresponding primary antibody was used as a negative control for


https://dx.doi.org/10.1021/acsabm.0c01627
ACS Appl. Bio Mater. 2021, 4, 3304−3319

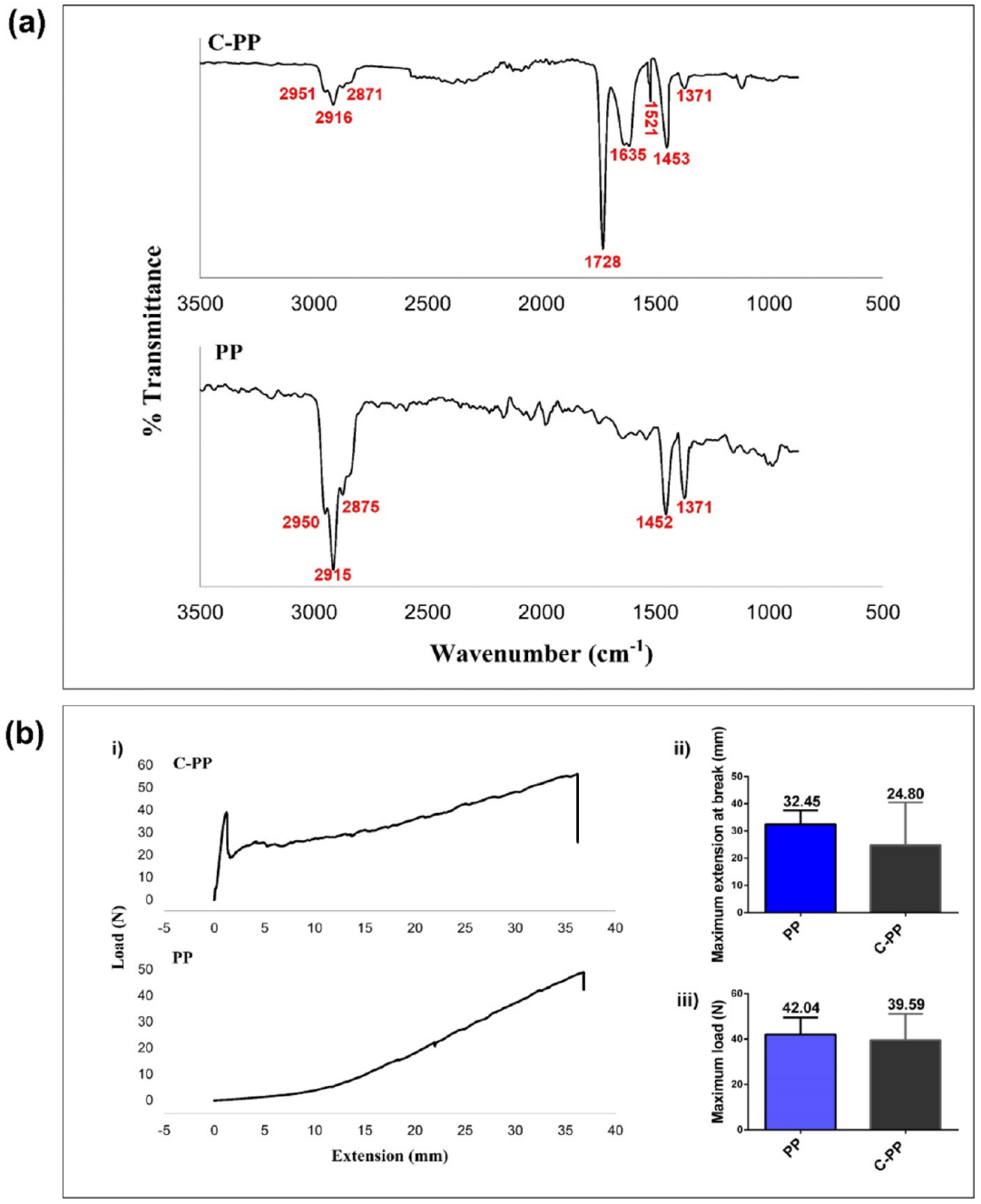


**Figure 3.** Chemical composition and mechanical strength of PP and C-PP meshes. (a) Fourier transform infrared spectra of a PP and a C-PP mesh (b-i) Line graph depicting load vs. extension characteristics of PP and C-PP meshes. (b-ii,iii) Bar diagrams representing the maximum extension and maximum load on the meshes at break ($n$ = 4). PP: polypropylene; C-PP: CECM hydrogel-coated polypropylene mesh. The results were analyzed by two-way ANOVA. Error bars represent mean ± SEM.

every immunohistochemistry procedure. All these reactions were detected using a supersensitive polymeric HRP detection system (Bio Genex Laboratories, USA) and counterstained with Harris's hematoxylin. The images were captured using a DP71 camera loaded onto a BX51 microscope (Olympus Corporation, Japan).

**2.6. Statistical Analysis.** Results were presented as mean ± standard error (SEM) unless otherwise specified and analyzed using Graphpad Prism 6.01 software. Comparison between different groups was performed with two-tailed Student's $t$-test or two-way ANOVA. An $\alpha$ level of $p$-value $\leq 0.05$ was considered to indicate the significant difference between the groups.

## 3. RESULTS AND DISCUSSION

**3.1. Preparation and Characterization of the C-PP Mesh.** Earlier studies have adopted two major strategies, either chemical grafting[22,27,28] or physical methods,[10,11,29] for coating hydrogels onto PP meshes. Chemical grafting utilizes selected chemical cross-linking agents but may significantly modify the basic biomaterial properties of the polymer, especially biocompatibility.[30] Therefore, this study opted for dip-coating, a commonly used physical method known for its simplicity and reliability in modifying surface characteristics of many biomaterials including those of polymeric origin.[10,11,31] The


https://dx.doi.org/10.1021/acsabm.0c01627
ACS Appl. Bio Mater. 2021, 4, 3304−3319

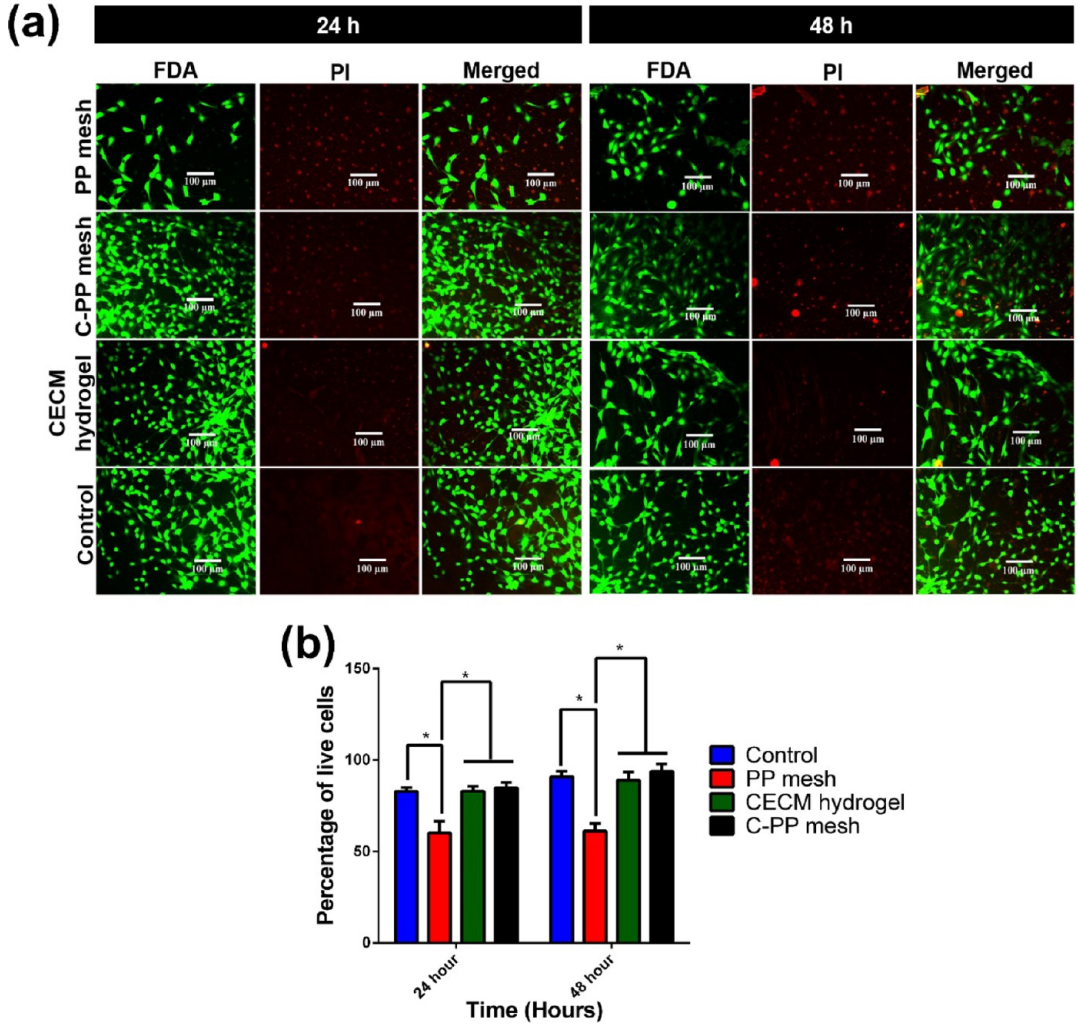


**Figure 4.** *In vitro* cell viability and biocompatibility studies of PP and C-PP meshes. Fluorescence microscopic images (a) depicting cell viability of C2C12 cells seeded on the CECM hydrogel, PP mesh, and C-PP mesh after 24 and 48 h and the corresponding quantitative data (b). PP: polypropylene; C-PP: CECM hydrogel-coated polypropylene mesh; CECM: cholecystic ECM; FDA: fluorescein diacetate; PI: propidium iodide. Magnification = 20×. The results were analyzed by two-way ANOVA (*$p$-value < 0.05). Error bars represent mean ± SEM, $n$ = 3.

biomaterial properties and biocompatibility of the C-PP mesh were evaluated.

The CECM hydrogel coating appeared as a white layer, covering the knits of the original PP mesh (Figure 2a). The coating resulted in an increase in the thickness of the original PP mesh from 0.33 to 0.64 ± 0.06 mm and the weight from 20 to 28 mg. The scanning electron micrographs confirmed the knitted structure, made of monofilament PP yarn. The CECM hydrogel coating completely masked the PP mesh fibers (Figure 2b). The coating was continuous and uniform between the PP mesh fibers. The FTIR spectrum of the original PP mesh had distinct absorption peaks of the methyl groups (2950, 2875, and 2915 $cm^{-1}$) and the alkane groups (1452 and 1371 $cm^{-1}$).[32] The C-PP mesh had all these peaks in addition to the characteristic peaks of collagen at 1628 $cm^{-1}$ (amide I) and 1522 $cm^{-1}$ (amide II) of the CECM[16] as well as a peak at 1727 $cm^{-1}$ representing the C═O stretch of PEGDA, the gelling agent in the original CECM hydrogel (Figure 3a).[21] These observations indicated a satisfactory coating of the CECM hydrogel over the PP mesh.

**3.2. Mechanical Property Evaluation.** A mismatch in mechanical strength between hernia repair materials and the host tissue may contribute to graft failure.[33] Therefore, despite the non-availability of any well-defined standard values, all hernia mesh designs place considerable emphasis on tensile strength. In this study, the maximum extension of the commercially available PP mesh was 32.46 mm at a load of 42.06 N and that of the C-PP mesh was 24.81 mm with a load of 39.59 N (Figure 3b). The reduction in the mechanical strength of the C-PP mesh was obviously due to the perceived increase in thickness/weight of the meshes because of the coating, leading to a variation in extension at longitudinal and transverse directions.[28,34] However, the observed reduction of the maximum extension or maximum load was not statistically significant (Figure 3b), indicating that the hydrogel coating did not modify the original mechanical properties of the PP mesh.

**3.3. Nonenzymatic Degradation of the C-PP Mesh.** The degradation behavior of the meshes was studied in PBS, a medium simulating physiological conditions.[35] The percentage degradation of PP mesh was "0" at all the evaluated time points. The C-PP mesh degradation started at 4 weeks (1.05%) and significantly increased at 8 (7.37%) and 16 (13.8%) weeks (Figure S3). The degradation of the hydrogel alone was 3.71 ± 1.45% at 4 weeks, which gradually increased to 25.81 ± 8.6 and 48.31 ± 14.02% at 8 and 16 weeks, respectively (Figure S3). As


https://dx.doi.org/10.1021/acsabm.0c01627
ACS Appl. Bio Mater. 2021, 4, 3304−3319

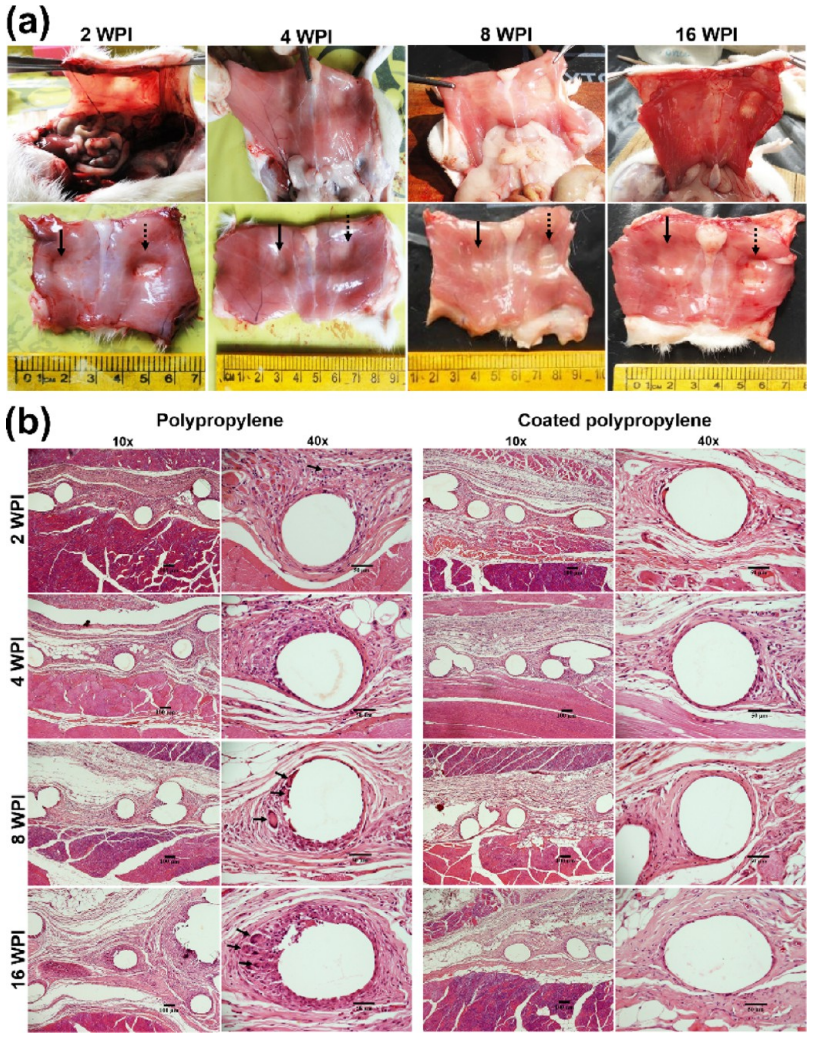


**Figure 5.** Gross evaluation and hematoxylin and eosin staining. (a) Gross appearances of the implants retrieved from the rat abdominal wall after 2, 4, 8, and 16 WPI. Black arrows indicate the C-PP mesh graft implanted on the left, and dotted black arrows indicate the PP mesh graft implanted on the right side of animals. (b) Histologic appearance of mesh grafts after 2, 4, 8, and 16 weeks of *in vivo* implantation with mild to moderate foreign body giant cells (black arrow). PP: polypropylene; C-PP: CECM hydrogel-coated polypropylene.

the bare PP mesh was non-degradable, the observed degradation was certainly due to the degradation of the coated hydrogel. UV−visible spectroscopy analysis was conducted in the C-PP mesh extracts to confirm whether the degrading components were part of the CECM hydrogel or not. The sharp peaks at 203 and 205 nm observed in the spectrum in the C-PP mesh extracts at 8 and 16 weeks (Figure S3) were indicative of collagen,[36] the major constituent of the ECM hydrogels.[37]

**3.4. *In Vitro* Biocompatibility Evaluation of the C-PP Mesh.** In view of the potential skeletal muscle tissue engineering application of the C-PP, the present study used C2C12 mouse skeletal myoblasts as the choice of the cells for all *in vitro* biological evaluations. Four test procedures were conducted for evaluating the cell viability, cell adhesion, cell proliferation, and *in vitro* biocompatibility. All test results indicated biocompatibility of the C-PP mesh with the PP mesh.

First, the results of live/dead staining (Figure 4a) indicated that, even after 48 h, 88.94 and 93.99% C2C12 cells were viable on the C-PP mesh and the CECM hydrogel, respectively, whereas only 36.15% cells were viable on the PP mesh (Figure 4b). The second test was a qualitative test that revealed the cytoskeletal distribution of C2C12 cells, which demonstrated cell adherence efficiency. The spindle morphology of the myoblast cells grown on all the test materials was preserved, suggesting their physiological status. The observation indicated that the materials did not cause any toxicity to the cells. Even though only a few cells adhered to the PP mesh (Figure S4), the adhered cells were viable and maintained a spindle morphology. Considering that the commercial PP mesh had a knitted surface architecture, which could potentially limit cell attachment and viability of the cultured skeletal myoblast cells,[38] the observation did not demand any further attention. Third, the results of cell cycle analysis by flow cytometry suggested that none of the test materials influenced the progression of the cell cycle (Figure S5). The percentage of cells in G0, G1, S, and G2/M phases of the cell cycle was similar in all the evaluated test samples (Figure S5). Finally, *in vitro* biocompatibility of the C-PP mesh was assessed using the test on the extract method, as recommended in ISO standards.[24,39,40] The results indicated that the majority of cells were viable (Figure S6), implying the absence of leachable toxic substances in the test materials. The comparison with the predicate device permitted the deduction that the C-PP was a safe biomedical device.



https://dx.doi.org/10.1021/acsabm.0c01627
*ACS Appl. Bio Mater.* 2021, 4, 3304−3319

Table 1. Semiquantitative Parameters Studied for Evaluating Histopathology (Parameters as per ISO 10993, Part 6—2016)[a]

| experimental groups | PP mesh | | | | C-PP mesh | | | |
|---|---|---|---|---|---|---|---|---|
| | 2 WPI | 4 WPI | 8 WPI | 16 WPI | 2 WPI | 4 WPI | 8 WPI | 16 WPI |
| Cell Response | | | | | | | | |
| PMNL | 1 | 1 | 1 | 0.75 | 1 | 1 | 0.75 | 0.75 |
| lymphocytes | 1.25 | 1.25 | 1 | 0.825 | 1 | 1 | 0.75 | 0.76 |
| plasma cells | 1 | 0.75 | 0.75 | 0.75 | 1 | 0.75 | 0.75 | 0.75 |
| macrophages | 4 | 3.5 | 3.25 | 3 | 2.25 | 2 | 1.75 | 1.5 |
| giant cells | 2 | 1.5 | 1 | 2 | 0.75 | 1 | 0.75 | 0.75 |
| necrosis | 0 | 0 | 0 | 0 | 0 | 0 | 0 | 0 |
| subtotal I | 9.25 | 8.00 | 7.00 | 7.32 | 6.00 | 5.75 | 4.75 | 4.51 |
| Tissue Response | | | | | | | | |
| neovascularization | 1 | 2 | 3 | 4 | 2 | 2 | 4 | 4 |
| fibrosis | 3 | 3 | 4 | 4 | 1 | 2 | 3 | 3 |
| fatty infiltrate | 2 | 2 | 3 | 4 | 1 | 1 | 2 | 3 |
| subtotal II | 6 | 6 | 10 | 12 | 4 | 5 | 9 | 10 |
| total score = (2 x subtotal I) + subtotal II | 24.5 | 22 | 24 | 26.65 | 16 | 16.5 | 18.5 | 19.02 |
| comparative (reference vs test) reactivity score | | | | | 0 | 0 | 0 | 0 |

[a]All values represent mean ($n$ = 4) of the semi-quantitative score of the local tissue response as per ISO 10993 Part-6 (2016), local effects of implantation. PP: polypropylene mesh; C-PP: CECM hydrogel-coated polypropylene; PMNL: poly morpho nuclear leukocytes; WPI: weeks post-implantation. In the case of cell response, gradings were based on the number and distribution of cells (0 = 0 cell, 1 = 1−5 cells, 2 = 6−15 cells, 3 = heavy infiltration, and 4 = packed cells, represented as average of 5 fields at magnification, 400×). Severity of necrosis: grading is determined by the presence of cell debris and inflammation (0 = not present, l = minimally present, 2 = mild degree, 3 = moderate degree, and 4 = severe degree). Neovascularization: the extent measured as counts of the number of detectable vasculatures under a magnification of 400× (0 = no capillaries, l = l−3 capillaries, 2 = 4−7 capillaries, 3 = broad blood vessels, and 4 = extensive vascularization). Fibrosis measured as the thickness of the fibrous capsule, under a magnification of 400×, around the implant (0 = absent, 1 = 30 mm). Fatty infiltrate grading is determined by the amount of fatty tissue (0 = not present, 1 = minimally present, 2 = mild degree, 3 = moderate degree, and 4 = severe degree). Please see Tables S1−S4 for scores obtained for each animal.

**3.5. Animal Experimentation.** The rat partial-thickness abdominal wall skeletal muscle defect model was selected to meet the requirements of the twin objectives of the study. Primarily, it is an established model for evaluating abdominal hernia repair grafts.[11,15,28,41] Second, standard protocols for assessing biocompatibility and safety evaluation (ISO 10993-Part -6, 2016) recommend a study of the local pathological effects of implantation at the indented site of application in a suitable animal model.[15,25] Considering that hernia repair meshes are expected as long-term implants, the duration of the study period was 16 weeks, a commonly recommended duration.[42] Indeed, the duration of implantation was also in compliance with the above-mentioned standard protocols. The killing of animals at 2, 4, 8, and 16 weeks facilitated a fair comparison between the nature of the progressive skeletal muscle reaction caused by the bare PP mesh and the C-PP mesh.

*3.5.1. Gross Appearance of the Grafts.* There was no mortality, infection, adhesion, wound dehiscence, or other clinical complications in the animals after the surgery in any of the groups. Upon resection, the peritoneal surface of the explanted meshes had visible signs of neovascularization as early as 2 WPI in both groups, a gross evidence of the integration of the grafts with the skeletal muscles of the abdominal wall (Figure 5a). The density of blood vessels increased with time, but no quantification was performed. In addition, moderate thinning of the graft area was seen on the peritoneal surface of all the PP-grafted rats, which may be an indication of the differential healing reaction caused by the grafts. It can be criticized that the observed differential gross reaction is a "side effect" due to the preferential implantation of the PP meshes on the left side and the C-PP mesh on the right. This could be a limitation of the study. However, the attending veterinarian did not report any unusual signs of discomfort or postural abnormalities among the rats during the post-implantation experimental period. Therefore, it was assumed that the "side effect", if at all any, was negligible.

*3.5.2. Histomorphology of the Local Effects of Implantation.* The histomorphological observations provided insights into the nature of the local tissue reaction to the PP and C-PP grafts. The graft-induced reactions were essentially foreign body granulomatous inflammation contributed by mild to moderate infiltration of mononuclear cells, a variable number of foreign body giant cells (graded 0−4, per high power field, Table 1), and mild to moderate fibrosis (Figure 5b). The reaction was apparent as early as 2 WPI, and the severity of the reaction increased with time. The bare PP graft appeared to have caused a more severe reaction compared to the CECM hydrogel-modified graft, at all time points of the study. This variation prompted a quantitative assessment of the extent of variation in the nature of the tissue reaction between the two grafts.

In fact, a semi-quantitative histomorphological evaluation in experimental animals for local tissue responses at the intended site of application, in comparison with that of a predicate device, is the gold standard for assessing the potential safety of any biomaterial.[25,43] Here, in the absence of a commercial ECM-modified PP mesh capable of mitigating tissue reaction, the Trulene mesh served as the reference material and the predicate device for the evaluation. The semi-quantitative parameters evaluated are summarized in Table 1. The calculated 'reactivity score' as per the ISO standard[25] of the C-PP graft in comparison with PP was "0", at all the time points evaluated. Therefore, the biocompatibility of the C-PP mesh was deemed similar to that of the PP mesh, and the tested material was judged safe as a biomedical device.

Histomorphologically, despite the similarity in biocompatibility as per the ISO standard, the bare PP graft appeared to have caused a more severe tissue reaction compared to the C-PP graft. The perceived difference in the severity of the reaction


https://dx.doi.org/10.1021/acsabm.0c01627
ACS Appl. Bio Mater. 2021, 4, 3304−3319

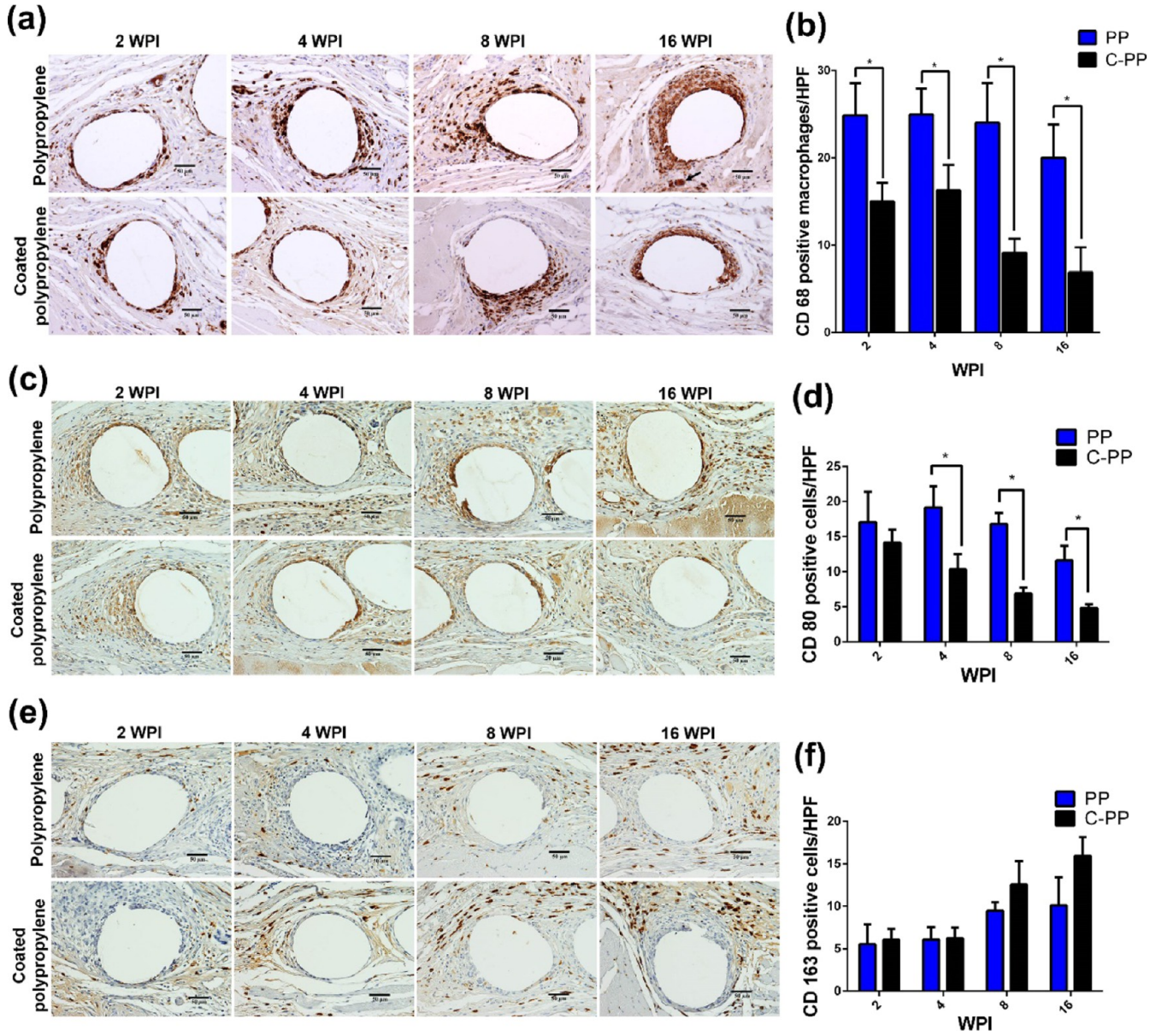


**Figure 6.** Immunohistochemistry for pan, M1, and M2 macrophages. Photomicrographs of immunohistochemistry and corresponding quantitative data for CD68 positive pan macrophages (a,b), CD80 positive M1 macrophages (c,d), and CD163 positive M2 macrophages (e,f) around PP and C-PP mesh grafts. PP: polypropylene; C-PP: CECM hydrogel-coated polypropylene; WPI: weeks post-implantation; HPF: high power field. The results were analyzed by two-way ANOVA (*$p$-value < 0.05). Error bars represent mean ± SEM, $n$ = 4.

warranted a detailed evaluation of the cell types participating in the tissue reaction. Considering that a PP graft-assisted skeletal muscle repair process is expected to contain a pool of locally proliferating cells, infiltrating cells of inflammation, angiogenesis, and formation of a fibrous tissue capsule around the mesh fibers,[1] in the present study, all these three components of the tissue reaction were studied in detail by histochemistry.

*3.5.3. Differential Inflammation Induced by PP and C-PP Grafts.* The reduced numbers of macrophages, lymphocytes, and foreign body giant cells from the *in vivo* biocompatibility evaluation (Table 1) gave room for suspecting the differential immunogenicity of the C-PP compared to the PP graft. It is known that biologic scaffold materials induce constructive tissue remodeling by inducing an M2 macrophage response.[44] Similarly, a preferred CD4 lymphocyte polarization has been observed in association with the graft acceptance reaction.[14] In this context, the nature of inflammation was evaluated by studying the distribution of CD68 (M0, pan-macrophage marker), CD80 (M1 macrophage marker), CD163 (M2 macrophage marker), CD4 (T helper cell marker), and CD8 (T cytotoxic cell marker) positive cells.

The immunohistochemical assessment indicated a modulated chronic inflammatory reaction around the C-PP graft. The number of CD68 positive pro-inflammatory macrophages was higher around the PP graft than around the C-PP graft at all time points of the study (Figure 6a,b), but the numbers consistently decreased over time. A similar trend was seen for the pro-inflammatory M1 macrophage tissue reaction between the groups (Figure 6c,d). Parallelly, a reverse trend was seen with respect to the infiltration of anti-inflammatory M2 macrophages, which increased over time (Figure 6e,f). Generally, rather than the actual numbers of M1 or M2 macrophages, the relative


https://dx.doi.org/10.1021/acsabm.0c01627
ACS Appl. Bio Mater. 2021, 4, 3304−3319

proportion of each of these cell types defines the nature of inflammation at a given reaction site,[14] probably by regulating the cytokine milieu of the microenvironment.[45] Normally, a larger proportion of M1 macrophages occurs during the pro-inflammatory phase, but M2 macrophages dominate in subsequent tissue remodeling phases of a wound-healing reaction.[46] Therefore, to ascertain the progress of the inflammation and the quickness of tissue remodeling reactions, the M1/M2 ratio was calculated for each time point of the evaluation (Figure 7). Perceptibly, pro-inflammatory reactions prevailed in early phases (2 and 4 WPI), followed by tissue remodeling reactions (8 and 16 WPI), around both the grafts. However, the severity of the reaction based on the M1/M2 ratio was much less around the C-PP graft at all time points, implying that the hydrogel coating significantly mitigated the severity of the inflammation and allowed the progression of a tissue remodeling reaction.

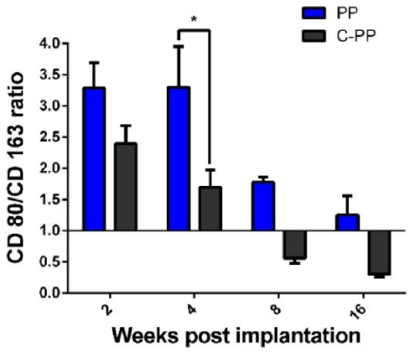


**Figure 7.** M1-to-M2 macrophage ratio. Bar graph representing the ratio of number of CD80 M1 positive macrophages to the number of CD163 positive M2 macrophages. Note the reversal of the ratio with a higher proportion of M2 macrophages. PP: polypropylene; C-PP: CECM hydrogel-coated polypropylene. The results were analyzed by two-way ANOVA (*$p$-value < 0.05). Error bars represent mean ± SEM, $n$ = 4.

This study also included an assessment of the relative proportion of CD4 and CD8 positive T-lymphocyte cells, which is an important determinant of the graft acceptance/rejection reaction.[47] These cell types play critical roles in conjunction with M1 and M2 macrophages in modulating chronic inflammation.[48] Having a role in adaptive immunity, CD4 positive T helper cells are limited to the major histocompatibility complex class II and act as helper cells for various immune responses, while CD8 positive T cytotoxic cells recognize antigens using the major histocompatibility complex class I and perform the cytotoxic function.[49] The number of CD4 positive cells continually increased during the study period from 2 WPI to 16 WPI around the grafts (Figure 8a,b). As expected, similar to the pattern of the M1 and M2 macrophage infiltration, the CD8 positive cells had a reverse trend compared to that of the CD4 positive T-helper cells (Figure 8c,d). The number of pro-inflammatory CD8 positive T cytotoxic cells decreased in the C-PP graft-implanted group with the advancement of time. However, the C-PP graft consistently stimulated higher numbers of T helper cells, which was also reflected in the CD4/CD8 ratio (Figure 9). It can be inferred that the CECM hydrogel coating on PP meshes mitigated the reaction by lowering the number of cytotoxic T cells and favoring a graft acceptance, at least from 4 weeks onward.

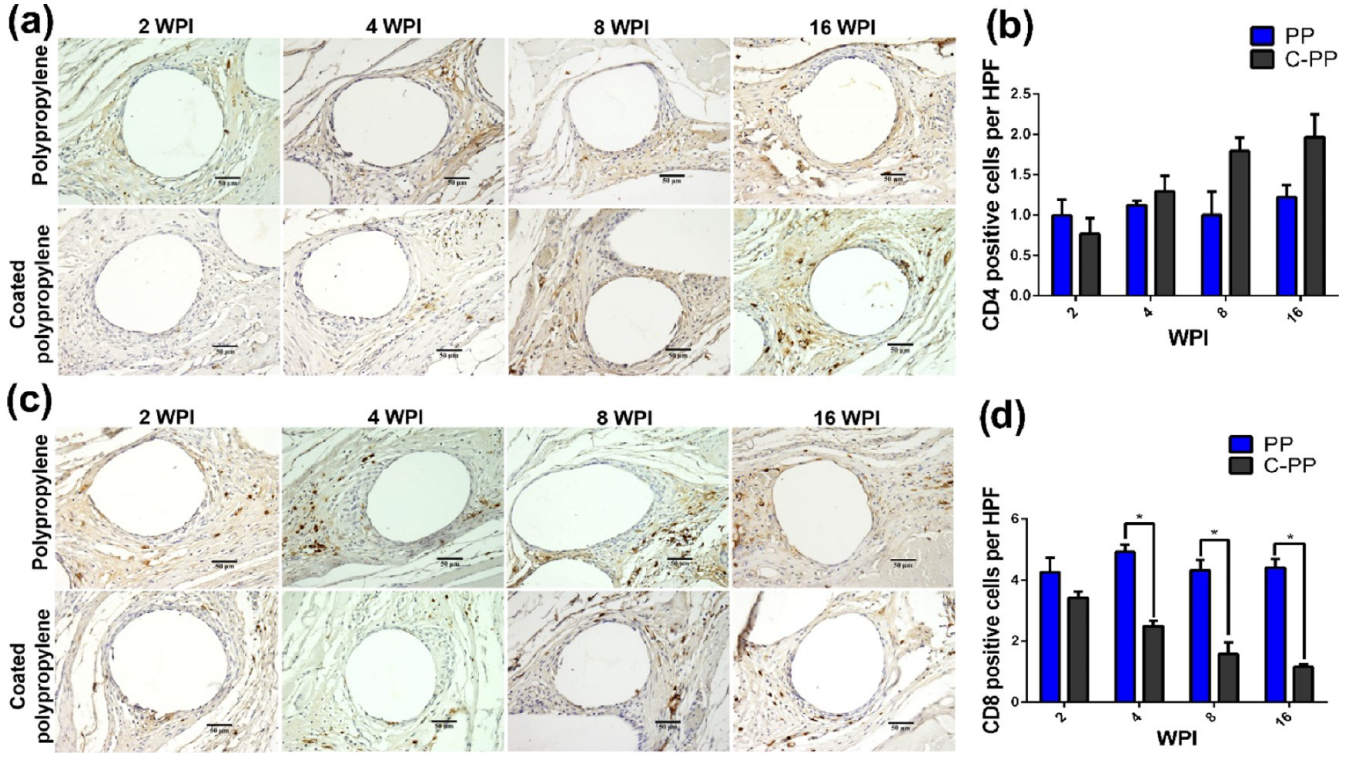


**Figure 8.** Immunohistochemistry for T helper and T cytotoxic lymphocytes. Photomicrographs of immunohistochemistry and corresponding quantitative data for CD4 lymphocytes (a,b), and CD8 lymphocytes (c,d) around PP and C-PP mesh grafts. PP: polypropylene; C-PP: CECM hydrogel-coated polypropylene; WPI: weeks post-implantation; HPF: high power field. The results were analyzed by two-way ANOVA (*$p$-value < 0.05). Error bars represent mean ± SEM, $n$ = 4.



https://dx.doi.org/10.1021/acsabm.0c01627
ACS Appl. Bio Mater. 2021, 4, 3304−3319

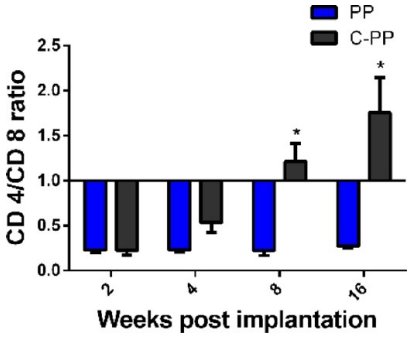


**Figure 9.** T helper to T cytotoxic lymphocyte ratio. Bar graph representing the ratio of number of CD4 T helper positive lymphocytes to the number of CD8 positive T cytotoxic lymphocytes. PP: polypropylene; C-PP: CECM hydrogel-coated polypropylene. The results were analyzed by two-way ANOVA (*$p$-value < 0.05). Error bars represent mean ± SEM, $n$ = 4.

*3.5.4. C-PP Graft Modulates Angiogenesis.* Adequate angiogenesis is essential in the remodeling phase of wound-healing responses.[8] Here, angiogenesis in the healing skeletal muscle was studied by immunostaining for two parameters: CD31 for immature blood vessels and ASMA for functional blood vessels. Immunohistochemistry for CD31 (a vascular endothelial cell marker) revealed sprouts of budding capillaries (Figure S7), while the ASMA detected mature blood vessels with well-differentiated myocytes in functional blood vessels (Figure S7). The number of CD31 as well as ASMA positive blood vessels progressively increased until 16 WPI in PP grafts (Figure S7). However, around the C-PP graft, angiogenesis remained similar at all the evaluated time points without any appreciable difference. Considering that excess angiogenesis has been associated with poor biocompatibility and intense foreign body reaction,[50] it was concluded that the C-PP graft did not stimulate any adverse reaction compared to the PP-graft. The progressive nature of angiogenesis around the PP graft suggested an extended tissue remodeling reaction or a delayed wound-healing process with persistent inflammation[8] compared to the tissue reaction around the C-PP grafts.

*3.5.5. Cell Proliferation and Fibroblast Infiltration.* In general, following an injury in any organ, tissue remodeling is contributed by regenerative responses of the parenchyma and the reparative process of the connective tissue.[51] However, following tissue injury in skeletal muscles, the terminally differentiated rhabdomyocytes in the G0 phase of the cell cycle[52] may not mount any significant regenerative response, and a reparative fibroblastic reaction dominates.[53] Therefore, the distribution of fibroblasts and the extent of cell proliferation in the histology sections were evaluated by immunostaining for vimentin and PCNA (Figure S8).

The density of vimentin positive cells was higher around both the grafts than that in normal tissues. Although vimentin is known as a fibroblast intermediate filament protein,[54] in reality, vimentin immunoreactivity occurs in a wide range of connective tissue cells, including endothelial cells, inflammatory cells, and fibroblasts.[55] Therefore, a quantitative estimate of the number of fibroblasts was not performed in this study, but the number of fibroblasts around both the grafts appeared similar (Figure S8).

The PCNA immunostaining (Figure S8) detected many proliferating cells in the reaction zone around the grafts; most of these are likely to be fibroblasts. Unfortunately, this study did not include a double immunohistochemistry reaction for identifying the actual number of proliferating fibroblasts. Nevertheless, the number of cells with proliferative potential appeared higher around PP grafts at all the evaluated time points (Figure S8). The observations suggested induction of a differential fibroblastic reaction by the grafts, possibly reinforcing the contention that the two grafts caused a differential cellular reaction in the skeletal muscles under repair. This observation demanded a study of the nature of fibrosis around the grafts.

*3.5.6. C-PP Graft Mitigated the Fibrotic Reaction.* All fibrotic reactions have a cellular and an acellular component.[53] This study investigated the differential nature of both these components around PP and C-PP. The most important cell types in a fibrotic reaction is certainly the fibroblast,[56] but myofibroblasts,[57] a transdifferentiated phenotype of disputed origin, which has contractile property, is also known to orchestrate the pathogenesis of fibrotic reactions in many lesions.[58] In addition, cells participating in inflammation, especially macrophages, have a pivotal role in modulating the local fibroblast function in the foreign body reaction.[59] As discussed earlier, there was no difference in the number of fibroblasts in the tissue reaction consequent to the implantation of PP and C-PP.

The distribution of ASMA positive myofibroblasts also appeared similar in both the graft-implanted groups at all the evaluated time points (Figure S7). In a wound-healing reaction, myofibroblasts gradually increase in number with the advancement of inflammation and as required for aiding contraction.[58] After a peak, their number decreases with the progression of the tissue remodeling phase.[60] In this study, the number of ASMA positive myofibroblasts was the highest by 2 WPI in both the groups and decreased thereafter. The observation indicated that the hydrogel coating on PP did not modulate the tissue contraction at the reaction site.[60]

Although there was no perceptible difference with respect to the numbers of fibroblasts or myofibroblasts in the tissue reactions, as discussed earlier, there were significant differences in the infiltration of lymphocytes and macrophages in the reaction zone. Considering that macrophages are known to regulate the acellular component of fibrotic reactions,[61] the investigators examined the nature of the acellular component in the skeletal muscle reaction to the PP and C-PP grafts.

The deposition of collagen around biomaterials is known as fibrotic encapsulation.[59] Normally, as the age of the lesion matures, the thickness of the fibrotic capsule increases with continual deposition of non-degradable collagen associated with a reduction in the number of fibroblasts.[53] We used Masson's trichrome (Figure 10a), which differentiated the blue colored collagen from pink colored skeletal muscle in histology sections, and quantified them by stereology. The stereology data did not give absolute measurements but gave an estimate of the difference in the compactness of collagen. Progressive fibrosis (indicated by the total collagen in the reaction zone) was observed around both the grafts, but the extent of fibrosis was consistently higher around the PP graft compared to C-PP, at all the evaluated periods (Figure 10b), with variably thick fibrous capsules (Figure 10c). Around the PP mesh, the percentage fibrosis at 2 WPI was 23.74 ± 3.2%, which increased to 36.95 ± 3.6% by 16 WPI. The corresponding values for the C-PP mesh were 12.09 ± 4.4 and 22.03 ± 3.9%, respectively. Extensive fibrosis in hernia repair creates an impedance mismatch at the wound-healing interface between the abdominal wall muscles and the relatively weak herniated area, potentially resulting in


https://dx.doi.org/10.1021/acsabm.0c01627
ACS Appl. Bio Mater. 2021, 4, 3304−3319

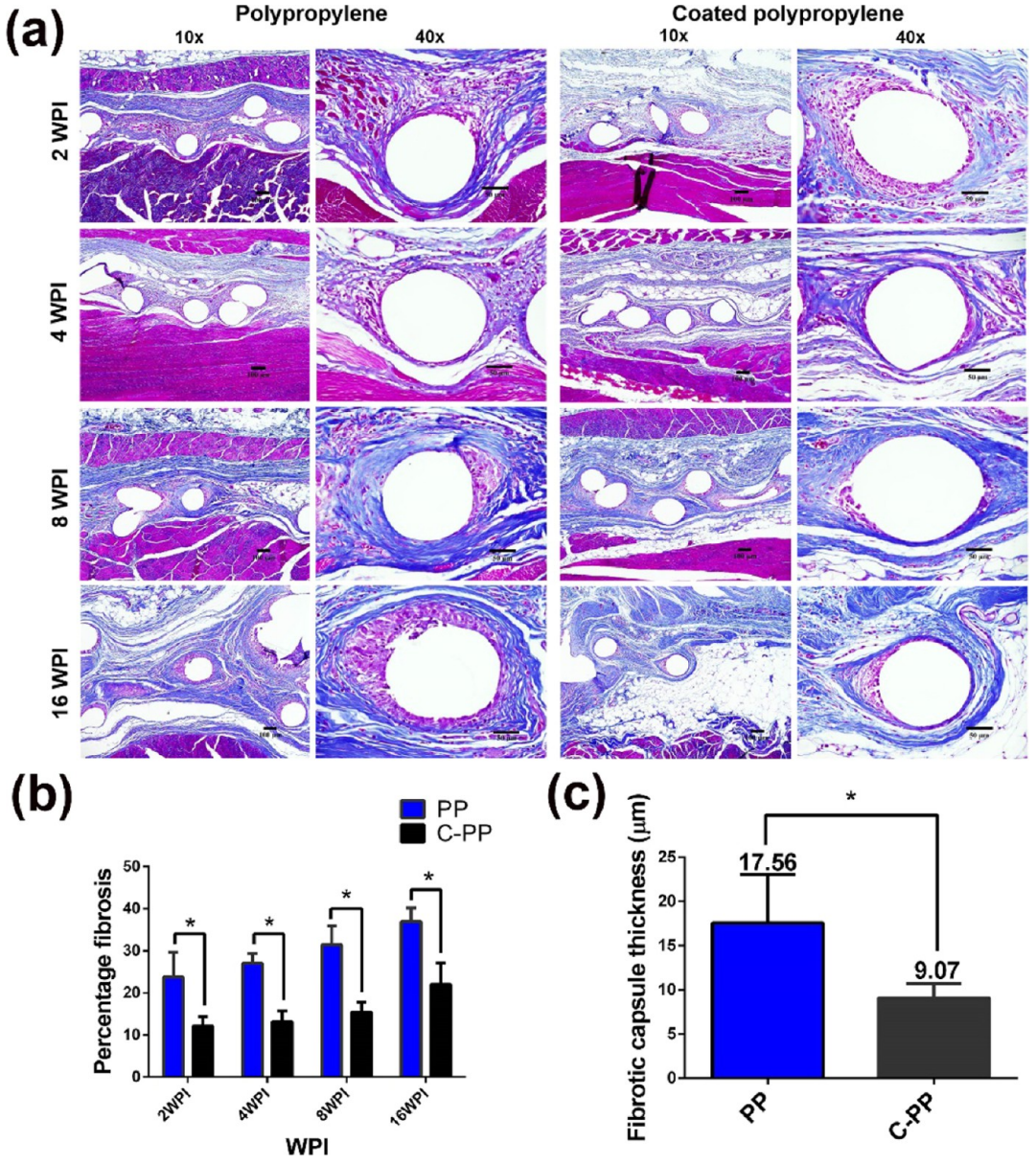


**Figure 10.** Masson's trichrome staining for collagen. (a) Representative light micrographs of Masson's trichrome stained sections made from PP and C-PP grafted animals. The blue-colored regions in the sections are indicative of collagen. (b) Bar diagram representing the percentage fibrosis. (c) Bar graph showing the thickness of the fibrous tissue capsule in PP and C-PP mesh grafts. PP: polypropylene; C-PP: CECM hydrogel-coated polypropylene; WPI: weeks post-implantation. The results were analyzed by two-way ANOVA (*$p$-value < 0.05). Error bars represent mean ± SEM.

mechanical wound failure and an increased risk of recurrent hernia formation.[62] The observation that the C-PP graft caused only about 2/3rd fibrosis compared to the PP graft raised a query regarding the nature of collagen types deposited around the grafts. Therefore, a detailed study of the different types of collagen that constituted the fibrotic reaction around the two grafts was conducted.

In reality, rather than the quantity of collagen, the type of collagen fibers constituting a reaction decides the nature of fibrosis at any tissue remodeling site, including reparative processes of abdominal skeletal muscle defects.[63] In fibrotic reactions, at least two sub-types of collagen can be expected, type I and type III collagen.[64] The former is essentially composed of highly cross-linked mature fibrillar collagen, relatively insensitive for enzymatic degradation compared to the latter, which is immature, amenable for degradation by matrix metalloproteinases.[65] The relative proportion of these collagen types defines the elasticity and mechanical strength of tissues.[66] The results of Herovici's staining reaction elucidated the differential nature of the collagen fiber in the skeletal muscle reaction around the grafts (Figure 11). The type I collagen deposition appeared rapid in the PP-induced reaction as early as 2 weeks, which remained stable during the rest of the experimental period until 16 WPI, but the deposition around the C-PP graft was minimal at 2 WPI, which gradually increased, and by 16 WPI, the proportion of type I collagen was similar around both grafts (Figure 12a). The observation suggested that the C-PP is capable of inducing fibrosis as good as that of the PP graft but requires a longer time for completing the reaction. Probably, this was a consequence of the intense pro-inflammatory reaction around the PP graft and a pro-graft-acceptance reaction around the C-PP mesh,[67] modulated by the different subsets of T


https://dx.doi.org/10.1021/acsabm.0c01627
ACS Appl. Bio Mater. 2021, 4, 3304−3319

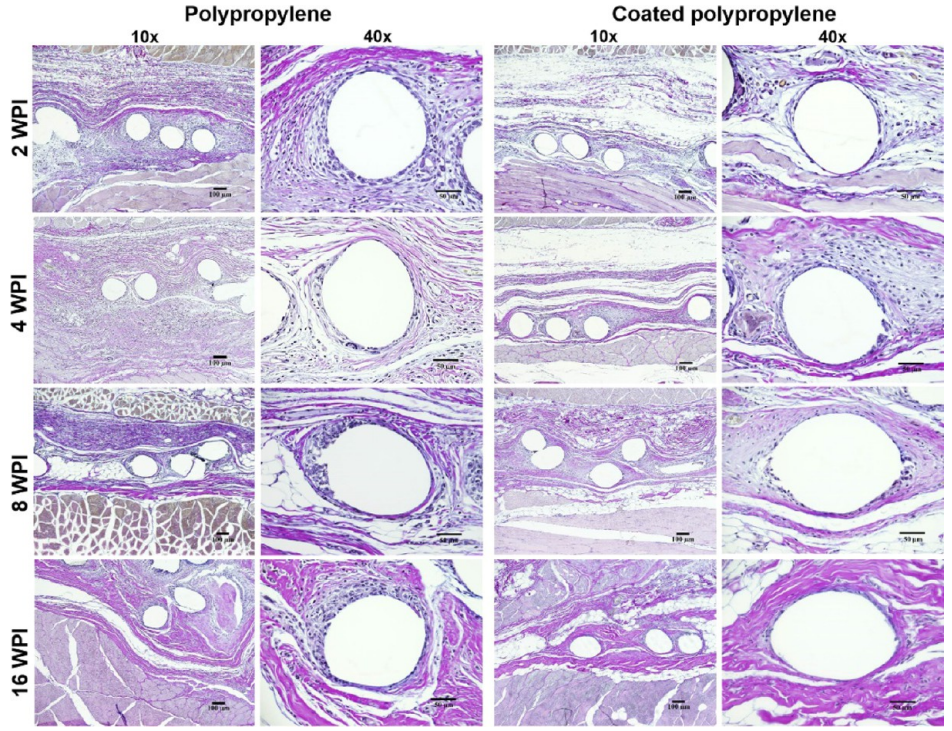


**Figure 11.** Herovici's polychromatic staining for type I and type III collagen. (a) Light micrographs of Herovici's stained sections made from PP and C-PP grafted animals. The blue- and pink-colored regions in these sections demonstrated type III immature and type I mature collagen, respectively. PP: polypropylene; C-PP: CECM hydrogel-coated polypropylene; WPI: weeks post-implantation.

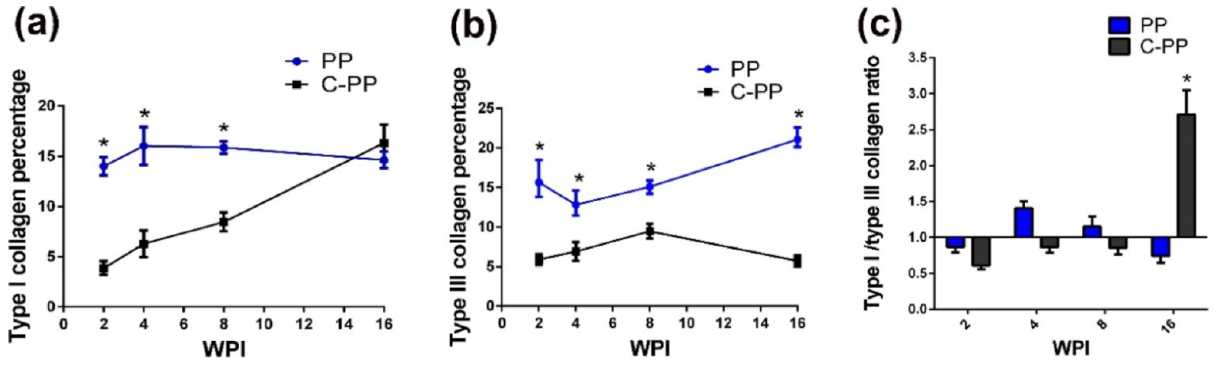


**Figure 12.** Quantification of collagen types from Herovici's polychromatic staining. Line graph representing the percentage area occupied by type I collagen (a) and type III collagen (b) determined from histology sections (see Figure 11) and a bar diagram showing an increase in the ratio of type I to III collagen in the C-PP-grafted group compared to that in the PP-grafted group. PP: polypropylene; C-PP: CECM hydrogel-coated polypropylene; WPI: weeks post-implantation. The results were analyzed by two-way ANOVA (*$p$-value < 0.05). Error bars represent mean ± SEM.

lymphocytes and macrophages. Moreover, the extent of type III collagen deposition was high around the PP graft compared to that around the C-PP graft (Figure 12b). The dissimilarity in the nature of collagen deposition was clearly appreciable in the ratio between the two types of collagen (Figure 12c). It is known that the lower ratios of collagen type I to collagen type III are associated with weaker and less mature scar tissue.[68] Insufficient scar composition with a lowered collagen type I/III ratio is a less durable reaction, which is frequently associated with recurring hernia formation.[66] Evidently, the excess collagen deposition observed around the PP mesh was due to the futile type III collagen. In fact, too much deposition of type III collagen surrounding a reaction zone of grafts is considered undesirable since it may lead to implant shrinkage, thick fibrotic capsule formation, and higher incidence of adhesions.[63,66,69] On the contrary, the C-PP grafts promoted the much-desired type I collagen, though the deposition was low at initial time points. Surely, C-PP had mitigated the tissue reaction by reducing the extent of inflammation through CD8 lymphocytes and M1 macrophages.

Contrastingly, the formation of a compact collagen-rich fibrous capsule is generally considered as a desirable reaction around many deep-tissue implants including PP hernia repair grafts, which is modulated by the nature of the associated inflammatory reaction and the implant surface chemistry.[62] A fibrous capsule was apparent as early as 2 WPI around both grafts and became prominent by 16 WPI (Figure 10c). The C-PP graft favored the formation of a relatively thin, less space occupying compact fibrotic capsule (9.07 ± 1.64 $\mu$m) when compared to the PP graft (17.56 ± 5.49 $\mu$m). Thus, it is certain that the C-PP-graft modulated a desirable fibrotic reaction compared to the PP graft.


https://dx.doi.org/10.1021/acsabm.0c01627
ACS Appl. Bio Mater. 2021, 4, 3304−3319

**3.6. Practical Implications of the Study.** In summary, although C-PP appeared biocompatible with PP, the nature of the inflammatory reaction, neovascularization, and collagen deposition around the two grafts were different. The initiation and progression of the healing reaction around the C-PP mesh was slower than that around the PP mesh. However, as a long-term implant, the end reaction was similar in both meshes. It can be speculated that the initial reaction of the C-PP mesh was contributed by the CECM hydrogel. Later, the gel might have got degraded, gradually exposing the PP mesh with the advancement of time, during which desirable inflammatory and fibrotic reactions were established around the C-PP. Surely, the CECM hydrogel coating mitigated the foreign body response to the polymeric mesh material. Significantly, it mitigated the pro-inflammatory surgical trauma at earlier phases and contributed to the predominance of the desirable compact type I collagen in subsequent stages of the healing reaction. Surely, the hydrogel coating made the tissue reaction milder in the skeletal muscle, but it was impossible to predict the extent of mesothelialization or the nature of intraperitoneal adhesion reactions had it been in contact with the peritoneal cavity. Experiments with a full-thickness abdominal defect animal model are needed to elucidate the potential of C-PP in modulating the nature of peritoneal reactions. Nevertheless, the C-PP mesh appears to be a promising biomedical device, especially as a skeletal muscle repair graft, which demands a low pro-inflammatory reaction without compromising the mechanical properties of PP.

## 4. CONCLUSIONS

Dip-coating was a satisfactory method for surface modification of the PP hernia repair mesh with the CECM hydrogel. The biocompatibility of the CECM hydrogel C-PP mesh was similar to the predicate device (Trulene) but induced a differential immunocompatibility reaction. The CECM hydrogel C-PP mesh mitigated the skeletal muscle tissue reaction by reducing the numbers of pro-inflammatory M1 macrophages and CD8 lymphocytes. The reduction in the chronic inflammatory response resulted in an altered fibrotic reaction, with abundance of type I collagen deposition, as ideally required for repairing skeletal muscle tissue defects.

## ■ ASSOCIATED CONTENT

### Supporting Information

The Supporting Information is available free of charge at https://pubs.acs.org/doi/10.1021/acsabm.0c01627.

Surgical implantation of grafts; sampling plan adopted for estimating the thickness of the fibrous tissue capsule around the mesh fiber; non-enzymatic degradation of PP and C-PP meshes; cell adhesion on PP and C-PP meshes; cell cycle analysis of C2C12 skeletal myoblasts on PP and C-PP meshes; MTT assay of CECM hydrogel extracts; immunohistochemistry for CD31 and $\alpha$-smooth muscle actin (ASMA); immunohistochemistry for vimentin and PCNA; and semi-quantitative scores for determining cellular response at 2, 4, 8, and 16 WPI presented in Table 1 of the main document (PDF)

## ■ AUTHOR INFORMATION


### Corresponding Author

**Thapasimuthu V. Anilkumar** − *Division of Experimental Pathology, Sree Chitra Tirunal Institute for Medical Sciences and Technology, Thiruvananthapuram 695012, India; School of Biology, Indian Institute of Science Education and Research—Thiruvananthapuram, Vithura 695551, India;* orcid.org/0000-0001-5594-877X; Email: tvanilkumar@sctimst.ac.in

### Authors

**Reshmi Raj** − *Division of Experimental Pathology, Sree Chitra Tirunal Institute for Medical Sciences and Technology, Thiruvananthapuram 695012, India*

**Sachin J. Shenoy** − *Division of In Vivo Models and Testing, Sree Chitra Tirunal Institute for Medical Sciences and Technology, Thiruvananthapuram 695012, India*

**Manjula P. Mony** − *Division of Experimental Pathology, Sree Chitra Tirunal Institute for Medical Sciences and Technology, Thiruvananthapuram 695012, India*

**Kanakarajan V. Pratheesh** − *Division of Experimental Pathology, Sree Chitra Tirunal Institute for Medical Sciences and Technology, Thiruvananthapuram 695012, India*

**Reshma S. Nair** − *Division of Experimental Pathology, Sree Chitra Tirunal Institute for Medical Sciences and Technology, Thiruvananthapuram 695012, India;* orcid.org/0000-0002-9296-0898

**Chandrika S. Geetha** − *Division of Experimental Pathology, Sree Chitra Tirunal Institute for Medical Sciences and Technology, Thiruvananthapuram 695012, India*

**Praveen K. Sobhan** − *Division of Tissue Culture, Sree Chitra Tirunal Institute for Medical Sciences and Technology, Thiruvananthapuram 695012, India*

**Chandramohanan Purnima** − *Division of Experimental Pathology, Sree Chitra Tirunal Institute for Medical Sciences and Technology, Thiruvananthapuram 695012, India*

Complete contact information is available at: https://pubs.acs.org/10.1021/acsabm.0c01627


### Notes

The authors declare no competing financial interest.

## ■ ACKNOWLEDGMENTS

R.R. acknowledges the support from the Kerala State Council for Science, Technology and Environment (KSCSTE—021/FSHP-LSS/2014) for the research fellowship. P.K.S. would like to thank the Science and Engineering Research Board (SERB) for Ramanujan Fellowship (SB/S2/RJN-152/2014).

## ■ REFERENCES


(1) Falco, E. E.; Roth, J. S.; Fisher, J. P. Skeletal Muscle Tissue Engineering Approaches to Abdominal Wall Hernia Repair. *Birth Defects Res., Part C* **2008**, *84*, 315−321.

(2) Bryan, N.; Ahswin, H.; Smart, N.; Bayon, Y.; Wohlert, S.; Hunt, J. A. The in Vivo Evaluation of Tissue-Based Biomaterials in a Rat Full-Thickness Abdominal Wall Defect Model. *J. Biomed. Mater. Res., Part B* **2014**, *102*, 709−720.

(3) Brown, C.; Finch, J. Which Mesh for Hernia Repair? *Ann. R. Coll. Surg. Engl.* **2010**, *92*, 272−278.

(4) Heymann, F.; von Trotha, K.-T.; Preisinger, C.; Lynen-Jansen, P.; Roeth, A. A.; Geiger, M.; Geisler, L. J.; Frank, A. K.; Conze, J.; Luedde, T.; Trautwein, C.; Binnebösel, M.; Neumann, U. P.; Tacke, F. Polypropylene Mesh Implantation for Hernia Repair Causes Myeloid Cell-Driven Persistent Inflammation. *JCI Insight* **2019**, *4*, No. e123862.

(5) Leber, G. E.; Garb, J. L.; Alexander, A. I.; Reed, W. P. Long-Term Complications Associated with Prosthetic Repair of Incisional Hernias. *Arch. Surg. Chic. Ill* **1998**, *133*, 378−382.

(6) Young, C. S.; Lyo, V.; Harris, H. W. Fasical Defect Size Predicts Recurrence Following Incisional Hernia Repair: A 7-Year, Single-Surgeon Experience. *Int. J. Abdom. Wall Hernia Surg.* **2020**, *3*, 11.
(7) Kalaba, S.; Gerhard, E.; Winder, J. S.; Pauli, E. M.; Haluck, R. S.; Yang, J. Design Strategies and Applications of Biomaterials and Devices for Hernia Repair. *Bioact. Mater.* **2016**, *1*, 2−17.
(8) Bredikhin, M.; Gil, D.; Rex, J.; Cobb, W.; Reukov, V.; Vertegel, A. Anti-Inflammatory Coating of Hernia Repair Meshes: A 5-Rabbit Study. *Hernia* **2020**, *24*, 1191−1199.
(9) Rastegarpour, A.; Cheung, M.; Vardhan, M.; Ibrahim, M. M.; Butler, C. E.; Levinson, H. Surgical Mesh for Ventral Incisional Hernia Repairs: Understanding Mesh Design. *Plast. Surg.* **2016**, *24*, 41−50.
(10) Wolf, M. T.; Carruthers, C. A.; Dearth, C. L.; Crapo, P. M.; Huber, A.; Burnsed, O. A.; Londono, R.; Johnson, S. A.; Daly, K. A.; Stahl, E. C.; Freund, J. M.; Medberry, C. J.; Carey, L. E.; Nieponice, A.; Amoroso, N. J.; Badylak, S. F. Polypropylene Surgical Mesh Coated with Extracellular Matrix Mitigates the Host Foreign Body Response. *J. Biomed. Mater. Res., Part A* **2014**, *102*, 234−246.
(11) Faulk, D. M.; Londono, R.; Wolf, M. T.; Ranallo, C. A.; Carruthers, C. A.; Wildemann, J. D.; Dearth, C. L.; Badylak, S. F. ECM Hydrogel Coating Mitigates the Chronic Inflammatory Response to Polypropylene Mesh. *Biomaterials* **2014**, *35*, 8585−8595.
(12) Freytes, D. O.; Martin, J.; Velankar, S. S.; Lee, A. S.; Badylak, S. F. Preparation and Rheological Characterization of a Gel Form of the Porcine Urinary Bladder Matrix. *Biomaterials* **2008**, *29*, 1630−1637.
(13) Grover, G. N.; Rao, N.; Christman, K. L. Myocardial Matrix-Polyethylene Glycol Hybrid Hydrogels for Tissue Engineering. *Nanotechnology* **2014**, *25*, 014011.
(14) Muhamed, J.; Revi, D.; Rajan, A.; Geetha, S.; Anilkumar, T. V. Biocompatibility and Immunophenotypic Characterization of a Porcine Cholecyst-Derived Scaffold Implanted in Rats. *Toxicol. Pathol.* **2015**, *43*, 536−545.
(15) Balakrishnan-nair, D. K.; Nair, N. D.; Venugopal, S. K.; Das, V. N.; George, S.; Abraham, M. J.; Eassow, S.; Alison, M. R.; Sainulabdeen, A.; Anilkumar, T. V. An Immunopathological Evaluation of the Porcine Cholecyst Matrix as a Muscle Repair Graft in a Male Rat Abdominal Wall Defect Model. *Toxicol. Pathol.* **2018**, *46*, 169−183.
(16) Anilkumar, T. V.; Vineetha, V. P.; Revi, D.; Muhamed, J.; Rajan, A. Biomaterial Properties of Cholecyst-Derived Scaffold Recovered by a Non-Detergent/Enzymatic Method. *J. Biomed. Mater. Res., Part B* **2014**, *102*, 1506−1516.
(17) Mony, M. P.; Anilkumar, T. V. Controlled Cross-Linking of Porcine Cholecyst Extracellular Matrix for Preparing Tissue Engineering Scaffold. *J. Biomed. Mater. Res., Part B* **2020**, *108*, 1057−1067.
(18) Muhamed, J.; Rajan, A.; Surendran, A.; Jaleel, A.; Anilkumar, T. V. Comparative Profiling of Extractable Proteins in Extracellular Matrices of Porcine Cholecyst and Jejunum Intended for Preparation of Tissue Engineering Scaffolds. *J. Biomed. Mater. Res., Part B* **2017**, *105*, 489−496.
(19) Revi, D.; Vineetha, V. P.; Muhamed, J.; Rajan, A.; Anilkumar, T. V. Porcine Cholecyst−Derived Scaffold Promotes Full-Thickness Wound Healing in Rabbit. *J. Tissue Eng.* **2013**, *4*, 2041731414556849.
(20) Revi, D.; Geetha, C.; Thekkuveettil, A.; Anilkumar, T. V. Fibroblast-Loaded Cholecyst-Derived Scaffold Induces Faster Healing of Full Thickness Burn Wound in Rabbit. *J. Biomater. Appl.* **2016**, *30*, 1036−1048.
(21) Raj, R.; Sobhan, P. K.; Pratheesh, K. V.; Anilkumar, T. V. A Cholecystic Extracellular Matrix-Based Hybrid Hydrogel for Skeletal Muscle Tissue Engineering. *J. Biomed. Mater. Res., Part A* **2020**, *108*, 1922−1933.
(22) Hu, W.; Zhang, Z.; Lu, S.; Zhang, T.; Zhou, N.; Ren, P.; Wang, F.; Yang, Y.; Ji, Z. Assembled Anti-Adhesion Polypropylene Mesh with Self-Fixable and Degradable in Situ Mussel-Inspired Hydrogel Coating for Abdominal Wall Defect Repair. *Biomater. Sci.* **2018**, *6*, 3030−3041.
(23) Kim, K. H.; Sederstrom, J. M. Assaying Cell Cycle Status Using Flow Cytometry. *Curr. Protoc. Mol. Biol.* **2015**, *111*, 28.
(24) Standard, I. *Biological Evaluation of Medical Devices. Part 5. Tests for Cyto-Toxicity: In Vitro Methods*; ISO 10993-5; Association for the Advancement of Medical Instrumentation: Arlington, VA, 2009. Int Stand ISO 10993-5 Biol Eval Med devices - Part 5 Tests Cytotox Vitr methods. 2009; 3 ed.
(25) Standard, I. *Biological Evaluation of Medical Devices. Part 6. Tests for Local Effects after Implantation*; ISO 10993-6; Association for the Advancement of Medical Instrumentation: Arlington, VA, 2016. Int Stand ISO 10993-6 Biol Eval Med devices - Part 6 Tests Local Effects Implantation. 2016; 3 ed.
(26) Turner, N. J.; Pezzone, M. A.; Brown, B. N.; Badylak, S. F. Quantitative Multispectral Imaging of Herovici's Polychrome for the Assessment of Collagen Content and Tissue Remodelling. *J. Tissue Eng. Regener. Med.* **2013**, *7*, 139−148.
(27) Hu, W.; Lu, S.; Zhang, Z.; Zhu, L.; Wen, Y.; Zhang, T.; Ji, Z. Mussel-Inspired Copolymer-Coated Polypropylene Mesh with Anti-Adhesion Efficiency for Abdominal Wall Defect Repair. *Biomater. Sci.* **2019**, *7*, 1323−1334.
(28) Ackermann, M.; Wang, X.; Wang, S.; Neufurth, M.; Schröder, H. C.; Isemer, F.-E.; Müller, W. E. G. Collagen-Inducing Biologization of Prosthetic Material for Hernia Repair: Polypropylene Meshes Coated with PolyP/Collagen. *J. Biomed. Mater. Res., Part B* **2018**, *106*, 2109−2121.
(29) Darzi, S.; Urbankova, I.; Su, K.; White, J.; Lo, C.; Alexander, D.; Werkmeister, J. A.; Gargett, C. E.; Deprest, J. Tissue Response to Collagen Containing Polypropylene Meshes in an Ovine Vaginal Repair Model. *Acta Biomater.* **2016**, *39*, 114−123.
(30) Oryan, A.; Kamali, A.; Moshiri, A.; Baharvand, H.; Daemi, H. Chemical Crosslinking of Biopolymeric Scaffolds: Current Knowledge and Future Directions of Crosslinked Engineered Bone Scaffolds. *Int. J. Biol. Macromol.* **2018**, *107*, 678−688.
(31) Hachim, D.; LoPresti, S. T.; Rege, R. D.; Umeda, Y.; Iftikhar, A.; Nolfi, A. L.; Skillen, C. D.; Brown, B. N. Distinct Macrophage Populations and Phenotypes Associated with IL-4 Mediated Immunomodulation at the Host Implant Interface. *Biomater. Sci.* **2020**, *8*, 5751−5762.
(32) Movasaghi, Z.; Rehman, S.; ur Rehman, D. I. Fourier Transform Infrared (FTIR) Spectroscopy of Biological Tissues. *Appl. Spectrosc. Rev.* **2008**, *43*, 134−179.
(33) Deeken, C. R.; Lake, S. P. Mechanical Properties of the Abdominal Wall and Biomaterials Utilized for Hernia Repair. *J. Mech. Behav. Biomed. Mater.* **2017**, *74*, 411−427.
(34) Sahoo, S.; DeLozier, K. R.; Erdemir, A.; Derwin, K. A. Clinically Relevant Mechanical Testing of Hernia Graft Constructs. *J. Mech. Behav. Biomed. Mater.* **2015**, *41*, 177−188.
(35) Jayasuriya, A. C.; Mauch, K. J. In Vitro Degradation Behavior of Chitosan Based Hybrid Microparticles. *J. Biomed. Sci. Eng.* **2011**, *04*, 383−390.
(36) Bächinger, H. P.; Mizuno, K. Collagen Triple Helix: Stability. *Wiley Encyclopedia of Chemical Biology*; American Cancer Society, 2008; pp 1−11.
(37) Saldin, L. T.; Cramer, M. C.; Velankar, S. S.; White, L. J.; Badylak, S. F. Extracellular Matrix Hydrogels from Decellularized Tissues: Structure and Function. *Acta Biomater.* **2017**, *49*, 1−15.
(38) Plencner, M.; Prosecká, E.; Rampichová, M.; East, B.; Buzgo, M.; Vysloužilová, L.; Hoch, J.; Amler, E. Significant Improvement of Biocompatibility of Polypropylene Mesh for Incisional Hernia Repair by Using Poly-ε-Caprolactone Nanofibers Functionalized with Thrombocyte-Rich Solution. *Int. J. Nanomed.* **2015**, *10*, 2635−2646.
(39) Keong, L. C.; Halim, A. S. In Vitro Models in Biocompatibility Assessment for Biomedical-Grade Chitosan Derivatives in Wound Management. *Int. J. Mol. Sci.* **2009**, *10*, 1300−1313.
(40) LI, W.; ZHOU, J.; XU, Y. Study of the in Vitro Cytotoxicity Testing of Medical Devices. *Biomed. Rep.* **2015**, *3*, 617−620.
(41) Wolf, M. T.; Daly, K. A.; Brennan-Pierce, E. P.; Johnson, S. A.; Carruthers, C. A.; D'Amore, A.; Nagarkar, S. P.; Velankar, S. S.; Badylak, S. F. A Hydrogel Derived from Decellularized Dermal Extracellular Matrix. *Biomaterials* **2012**, *33*, 7028−7038.
(42) Raghavendra, G. M.; Varaprasad, K.; Jayaramudu, T. Chapter 2—Biomaterials: Design, Development and Biomedical Applications. In *Nanotechnology Applications for Tissue Engineering*; Thomas, S.,


https://dx.doi.org/10.1021/acsabm.0c01627
ACS Appl. Bio Mater. 2021, 4, 3304−3319

Grohens, Y., Ninan, N., Eds.; William Andrew Publishing: Oxford, 2015; pp 21−44.
(43) Williams, D. F. Specifications for Innovative, Enabling Biomaterials Based on the Principles of Biocompatibility Mechanisms. *Front. Bioeng. Biotechnol.* **2019**, *7*, 255.
(44) Brown, B. N.; Ratner, B. D.; Goodman, S. B.; Amar, S.; Badylak, S. F. Macrophage Polarization: An Opportunity for Improved Outcomes in Biomaterials and Regenerative Medicine. *Biomaterials* **2012**, *33*, 3792−3802.
(45) Arango Duque, G.; Descoteaux, A. Macrophage Cytokines: Involvement in Immunity and Infectious Diseases. *Front. Immunol.* **2014**, *5*, 491.
(46) Ellis, S.; Lin, E. J.; Tartar, D. Immunology of Wound Healing. *Curr. Dermatol. Rep.* **2018**, *7*, 350−358.
(47) Porrett, P. M.; Lee, M. K.; Lian, M. M.; Wang, J.; Caton, A. J.; Deng, S.; Markmann, J. F.; Moore, D. J. A Direct Comparison of Rejection by CD8 and CD4 T Cells in a Transgenic Model of Allotransplantation. *Arch. Immunol. Ther. Exp.* **2008**, *56*, 193−200.
(48) Reichlin, M. The Role of Lymphocytes and Macrophages in the Immunological Response. *Arch. Intern. Med.* **1972**, *130*, 299−300.
(49) Couture, A.; Garnier, A.; Docagne, F.; Boyer, O.; Vivien, D.; Le-Mauff, B.; Latouche, J.-B.; Toutirais, O. HLA-Class II Artificial Antigen Presenting Cells in CD4+ T Cell-Based Immunotherapy. *Front. Immunol.* **2019**, *10*. DOI: DOI: 10.3389/fimmu.2019.01081.
(50) Modulevsky, D. J.; Cuerrier, C. M.; Pelling, A. E. Biocompatibility of Subcutaneously Implanted Plant-Derived Cellulose Biomaterials. *PLoS One* **2016**, *11*, No. e0157894.
(51) Krafts, K. P. Tissue Repair. *Organogenesis* **2010**, *6*, 225−233.
(52) Muhamed, J.; Revi, D.; Joseph, R.; Anilkumar, T. Phenotypic Modulation of Cell Types around Implanted Polyethylene Terephthalate Fabric in Rabbit Muscle. *Toxicol. Pathol.* **2013**, *41*, 497−507.
(53) Wynn, T. Cellular and Molecular Mechanisms of Fibrosis. *J. Pathol.* **2008**, *214*, 199−210.
(54) Danielsson, F.; Peterson, M.; Caldeira Araújo, H.; Lautenschläger, F.; Gad, A. Vimentin Diversity in Health and Disease. *Cells* **2018**, *7*, 147.
(55) Doppler, S. A.; Carvalho, C.; Lahm, H.; Deutsch, M.-A.; Dreßen, M.; Puluca, N.; Lange, R.; Krane, M. Cardiac Fibroblasts: More than Mechanical Support. *J. Thorac. Dis.* **2017**, *9*, S36−S51.
(56) Kendall, R. T.; Feghali-Bostwick, C. A. Fibroblasts in Fibrosis: Novel Roles and Mediators. *Front. Pharmacol.* **2014**, *5*, 123.
(57) Baum, J.; Duffy, H. S. Fibroblasts and Myofibroblasts: What Are We Talking About? *J. Cardiovasc. Pharmacol.* **2011**, *57*, 376−379.
(58) Bochaton-Piallat, M.-L.; Gabbiani, G.; Hinz, B. The Myofibroblast in Wound Healing and Fibrosis: Answered and Unanswered Questions. *F1000Research* **2016**, *5*. DOI: DOI: 10.12688/f1000research.8190.1.
(59) Anderson, J. M.; Rodriguez, A.; Chang, D. T. FOREIGN BODY REACTION TO BIOMATERIALS. *Semin. Immunol.* **2008**, *20*, 86−100.
(60) Ibrahim, M. M.; Chen, L.; Bond, J. E.; Medina, M. A.; Ren, L.; Kokosis, G.; Selim, A. M.; Levinson, H. Myofibroblasts Contribute to but Are Not Necessary for Wound Contraction. *Lab. Invest.* **2015**, *95*, 1429−1438.
(61) Simões, F. C.; Cahill, T. J.; Kenyon, A.; Gavriouchkina, D.; Vieira, J. M.; Sun, X.; Pezzolla, D.; Ravaud, C.; Masmanian, E.; Weinberger, M.; Mayes, S.; Lemieux, M. E.; Barnette, D. N.; Gunadasa-Rohling, M.; Williams, R. M.; Greaves, D. R.; Trinh, L. A.; Fraser, S. E.; Dallas, S. L.; Choudhury, R. P.; Sauka-Spengler, T.; Riley, P. R. Macrophages Directly Contribute Collagen to Scar Formation during Zebrafish Heart Regeneration and Mouse Heart Repair. *Nat. Commun.* **2020**, *11*, 600.
(62) Akilbekova, D.; Bratlie, K. M. Quantitative Characterization of Collagen in the Fibrotic Capsule Surrounding Implanted Polymeric Microparticles through Second Harmonic Generation Imaging. *PLoS One* **2015**, *10*, No. e0130386.
(63) Si, Z.; Bhardwaj, R.; Rosch, R.; Merten, P. R.; Klosterhalfen, B.; Klinge, U.; Rhanjit, B.; Rene, P. M. Impaired Balance of Type I and Type III Procollagen MRNA in Cultured Fibroblasts of Patients with Incisional Hernia. *Surgery* **2002**, *131*, 324−331.
(64) Witherel, C. E.; Abebayehu, D.; Barker, T. H.; Spiller, K. L. Macrophage and Fibroblast Interactions in Biomaterial-Mediated Fibrosis. *Adv. Healthcare Mater.* **2019**, *8*, 1801451.
(65) Xue, M.; Jackson, C. J. Extracellular Matrix Reorganization During Wound Healing and Its Impact on Abnormal Scarring. *Adv. Wound Care* **2015**, *4*, 119−136.
(66) Junge, K.; Klinge, U.; Rosch, R.; Mertens, P. R.; Kirch, J.; Klosterhalfen, B.; Lynen, P.; Schumpelick, V. Decreased Collagen Type I/III Ratio in Patients with Recurring Hernia after Implantation of Alloplastic Prostheses. *Langenbeck's Arch. Surg.* **2004**, *389*, 17−22.
(67) van Haaften, W. T.; Mortensen, J. H.; Karsdal, M. A.; Bay-Jensen, A. C.; Dijkstra, G.; Olinga, P. Misbalance in Type III Collagen Formation/Degradation as a Novel Serological Biomarker for Penetrating (Montreal B3) Crohn's Disease. *Aliment. Pharmacol. Ther.* **2017**, *46*, 26−39.
(68) Rosch, R.; Klinge, U.; Si, Z.; Junge, K.; Klosterhalfen, B.; Schumpelick, V. A Role for the Collagen I/III and MMP-1/-13 Genes in Primary Inguinal Hernia? *BMC Med. Genet.* **2002**, *3*, 2.
(69) Brown, S. R.; Melman, L.; Jenkins, E.; Deeken, C.; Frisella, M. M.; Brunt, L. M.; Eagon, J. C.; Matthews, B. D. Collagen Type I:III Ratio of the Gastroesophageal Junction in Patients with Paraesophageal Hernias. *Surg. Endosc.* **2011**, *25*, 1390−1394.


https://dx.doi.org/10.1021/acsabm.0c01627
*ACS Appl. Bio Mater.* 2021, 4, 3304−3319